Electronic Supplementary Information

for the manuscript entitled

Acceptorless oxidant-free dehydrogenation of amines catalyzed by Ru-hydride complexes of amide-acid/ester ligands

Samanta Yadav and Rajeev Gupta*

Department of Chemistry, University of Delhi, Delhi 110007, India

E-mail: rgupta@chemistry.du.ac.in

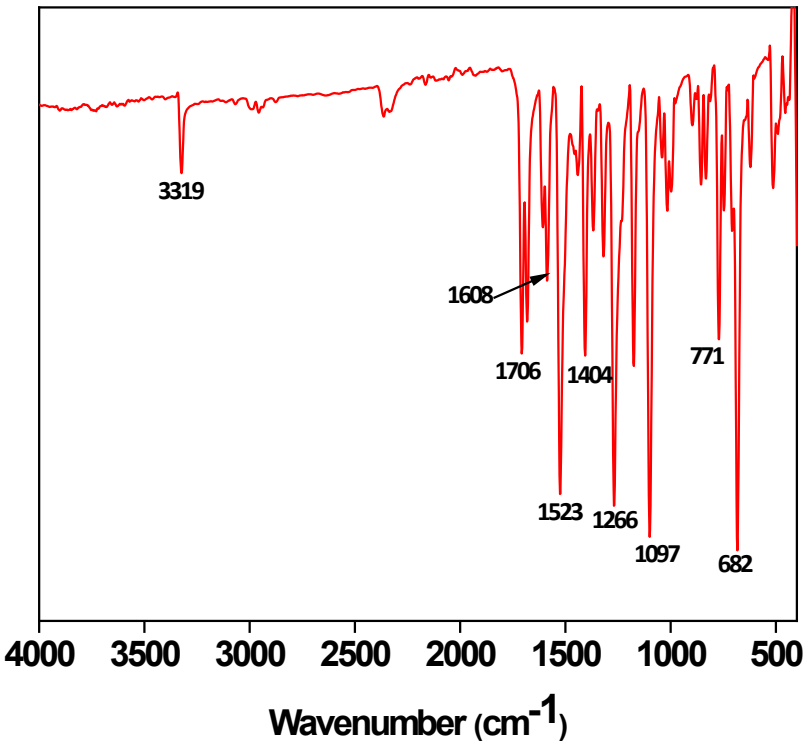

Figure S1. FTIR spectrum of ligand H**L1**.

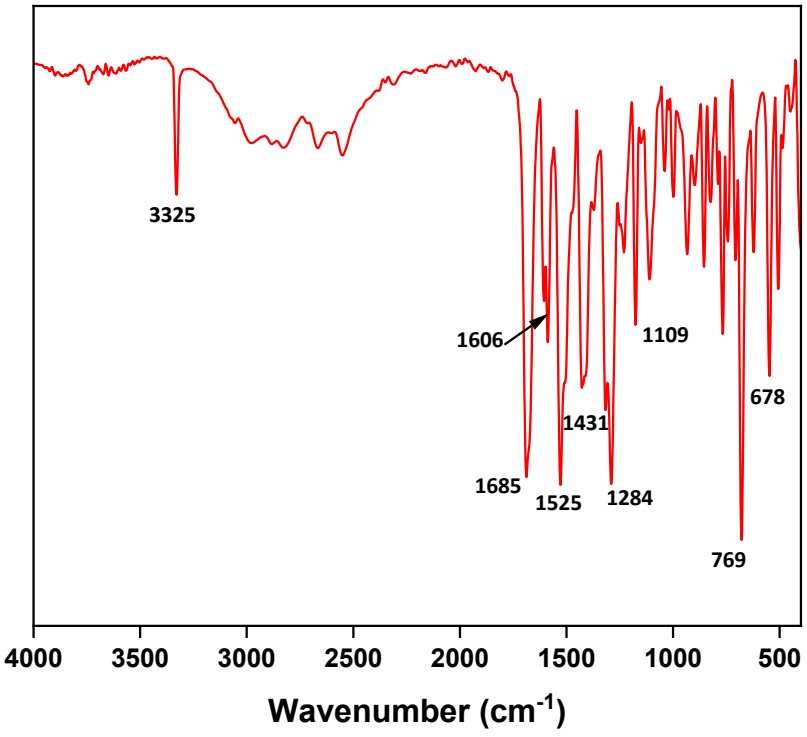

Figure S2. FTIR spectrum of ligand H**L2**.

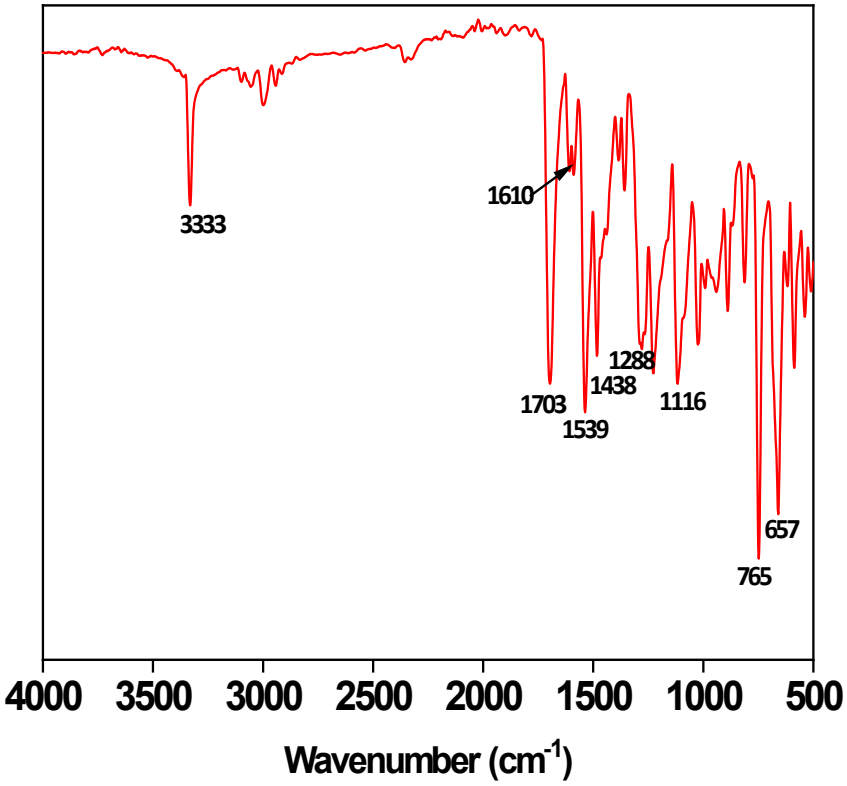

Figure S3. FTIR spectrum of ligand H**L3**.

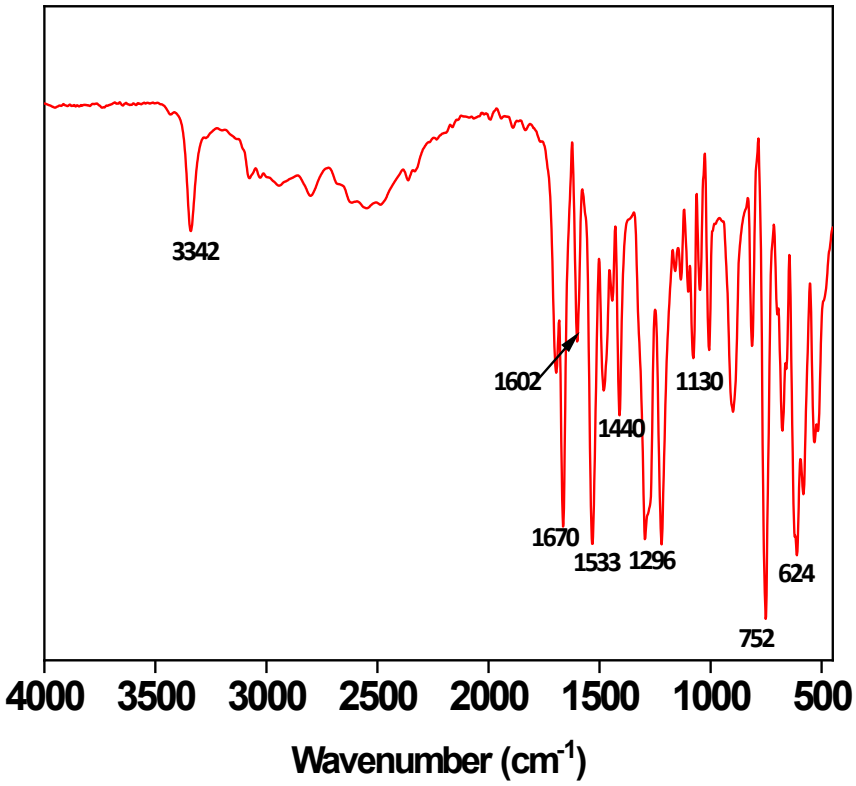

Figure S4. FTIR spectrum of ligand H**L4**.

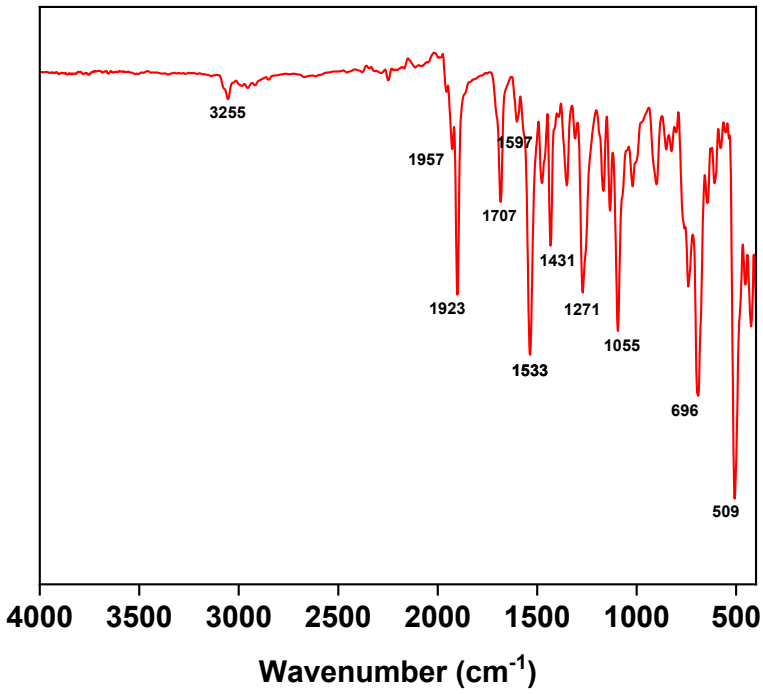

Figure S5. FTIR spectrum of complex **1**.

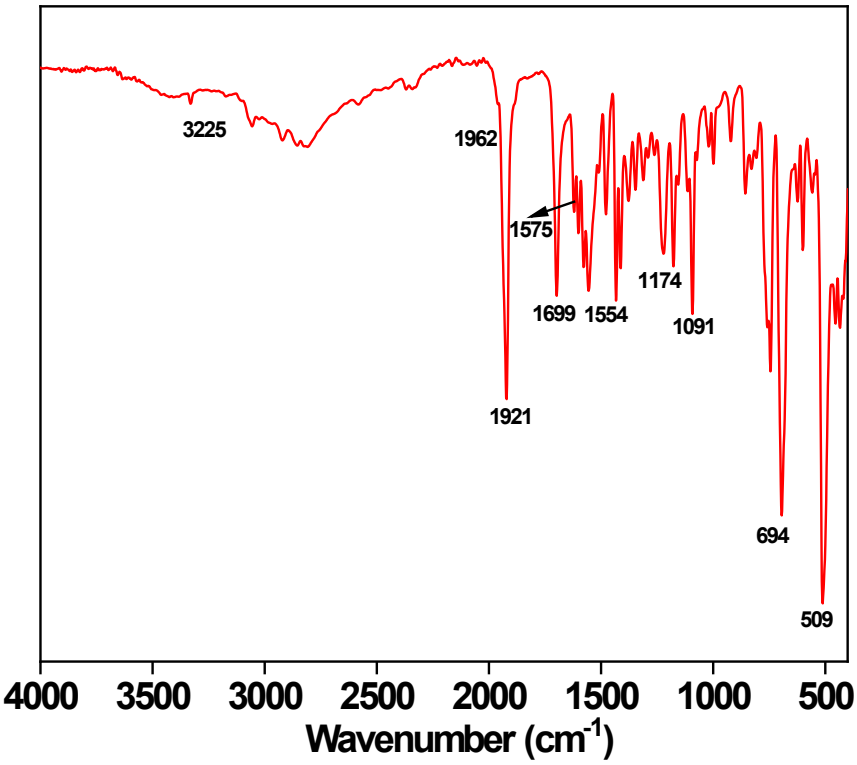

Figure S6. FTIR spectrum of complex **2**.

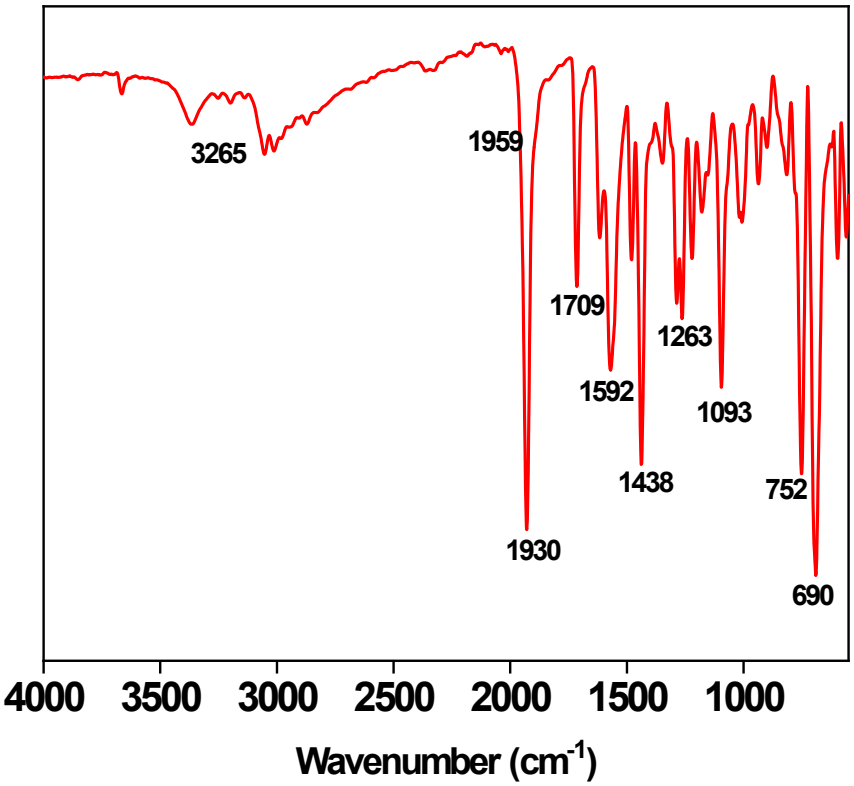

Figure S7. FTIR spectrum of complex **3**.

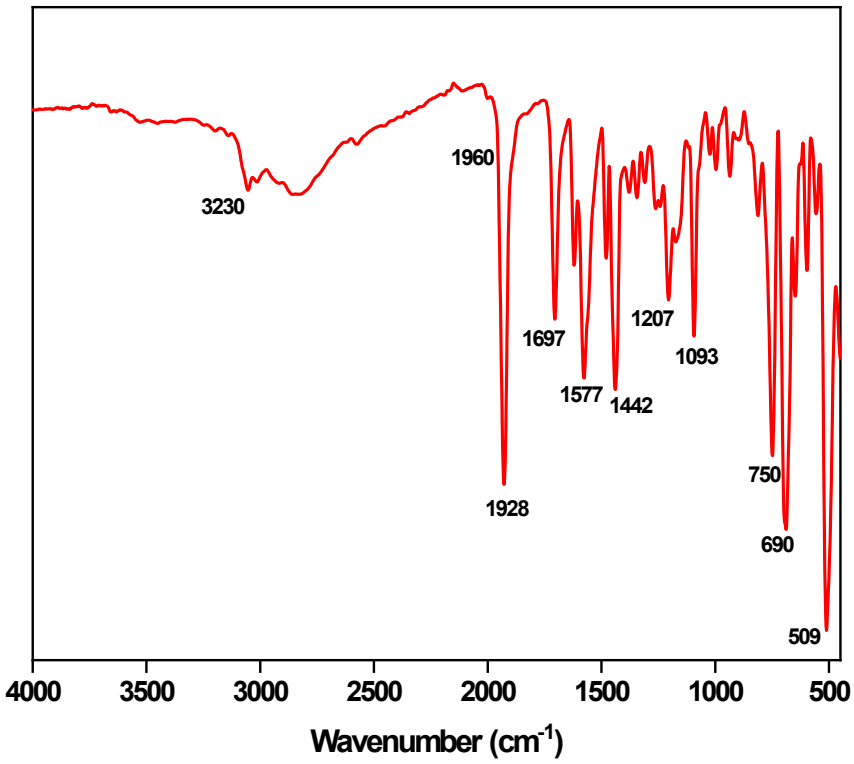

Figure S8. FTIR spectrum of complex **4**.

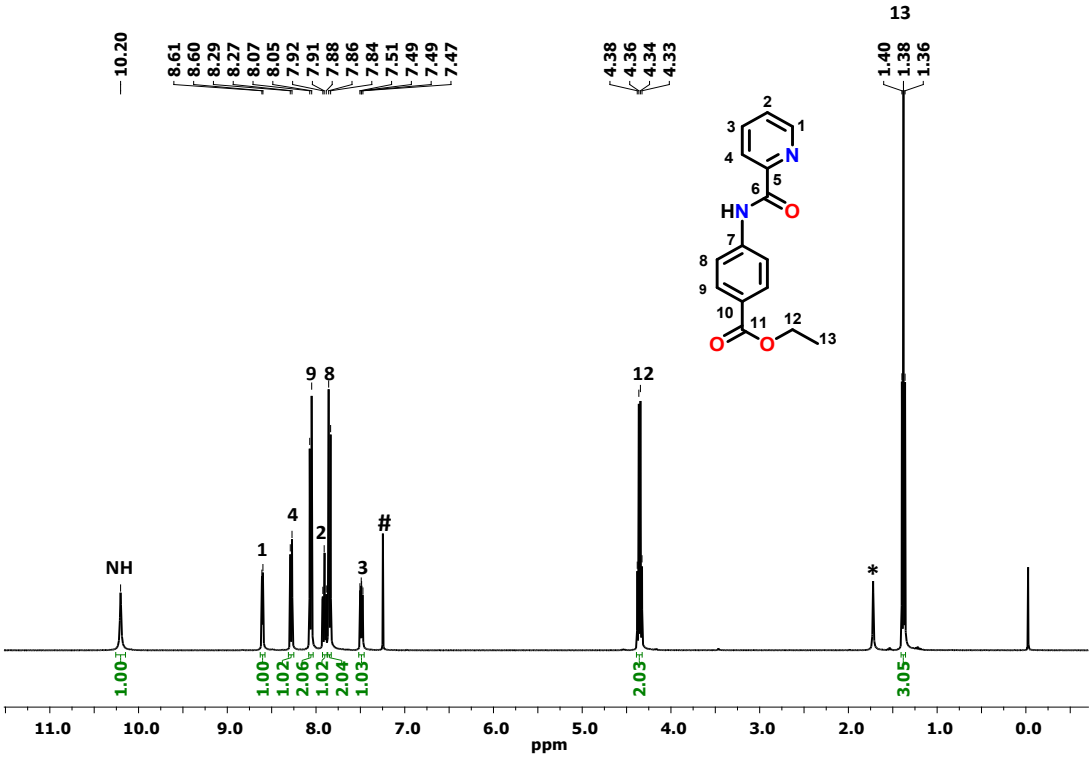

Figure S9. ^{1}H NMR spectrum of ligand H**L1** in $CDCl_3$. # and * represent $CDCl_3$ and residual solvent/ H_2O peak, respectively.

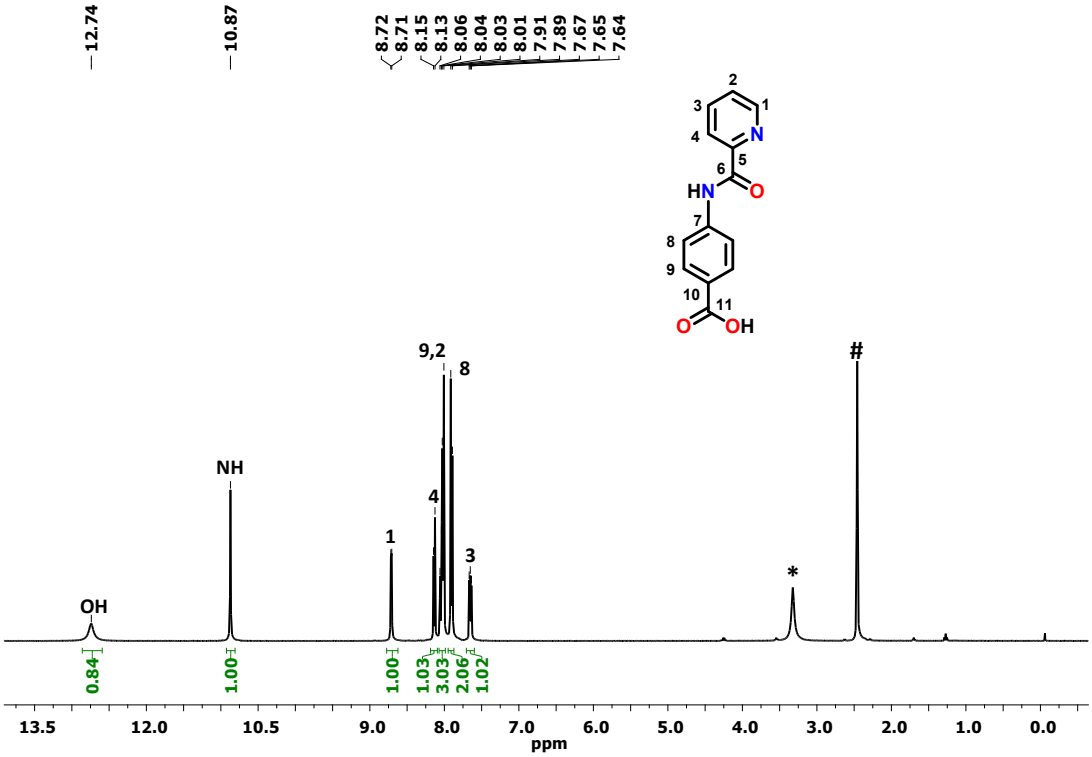

Figure S10. ^{1}H NMR spectrum of ligand H**L2** in DMSO-d_6. # and * represent DMSO-d_6 and residual solvent/ H_2O peak, respectively.

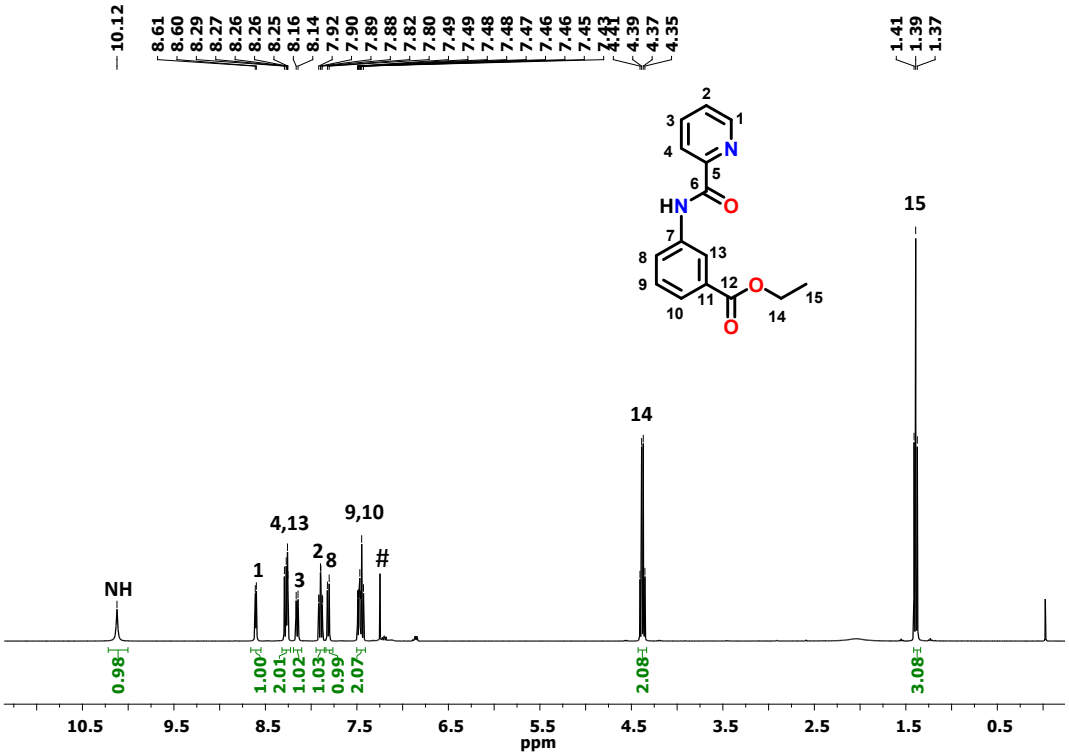

Figure S11. ^{1}H NMR spectrum of ligand H**L3** in $CDCl_3$. # Represents $CDCl_3$.

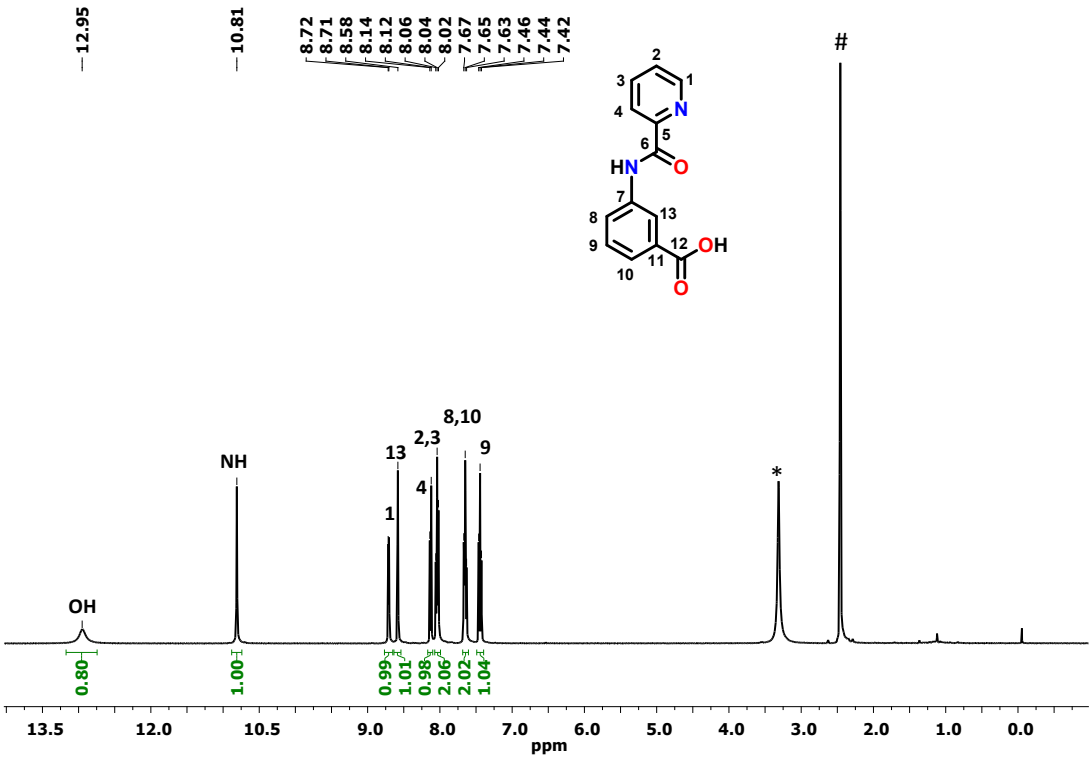

Figure S12. ^{1}H NMR spectrum of ligand H**L4** in DMSO-d_6. # and * represent DMSO-d_6 and residual solvent/ H_2O peak, respectively.

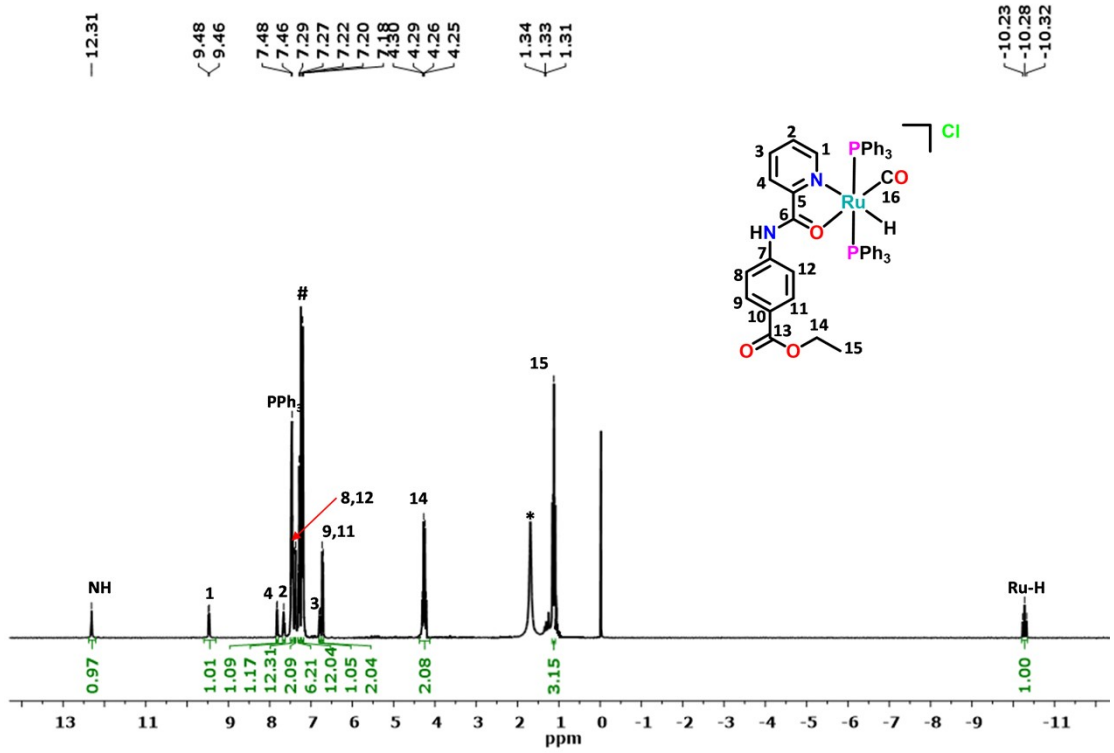

Figure S13. ^{1}H NMR spectrum of complex **1** in $CDCl_3$. # and * represent $CDCl_3$ and residual solvent/ H_2O peak, respectively.

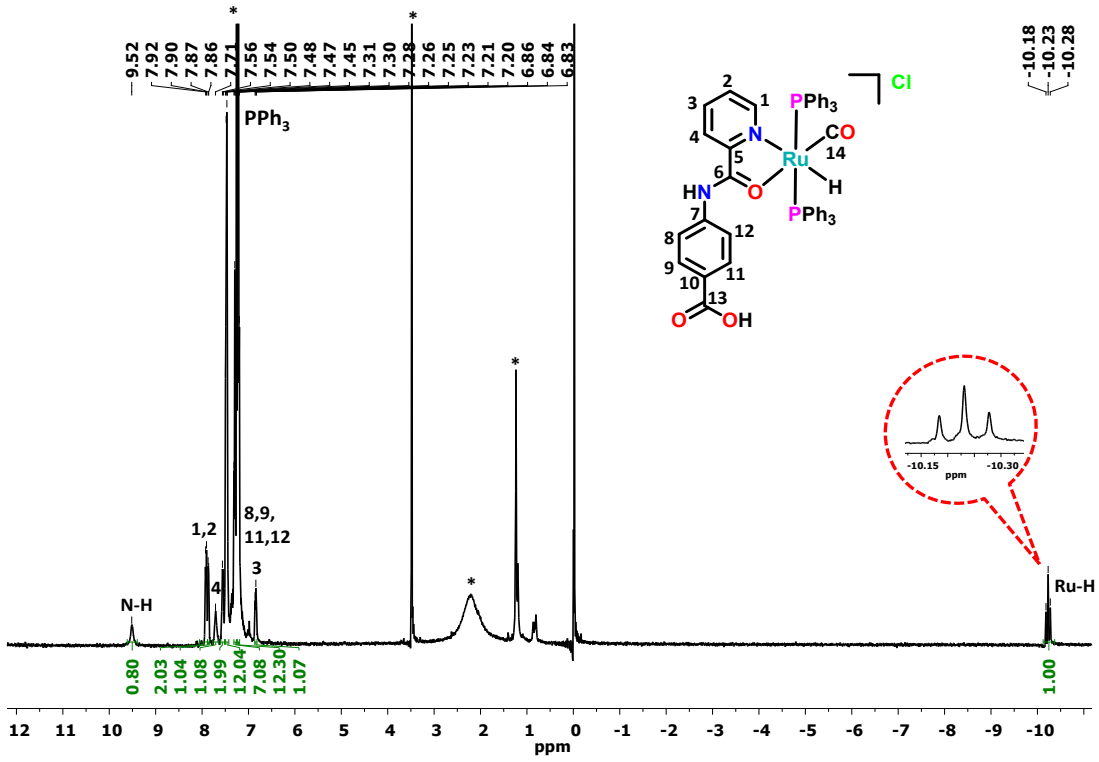

Figure S14. ^{1}H NMR spectrum of complex **2** in $CDCl_3$. * represents $CDCl_3$ /residual solvent/ H_2O peak.

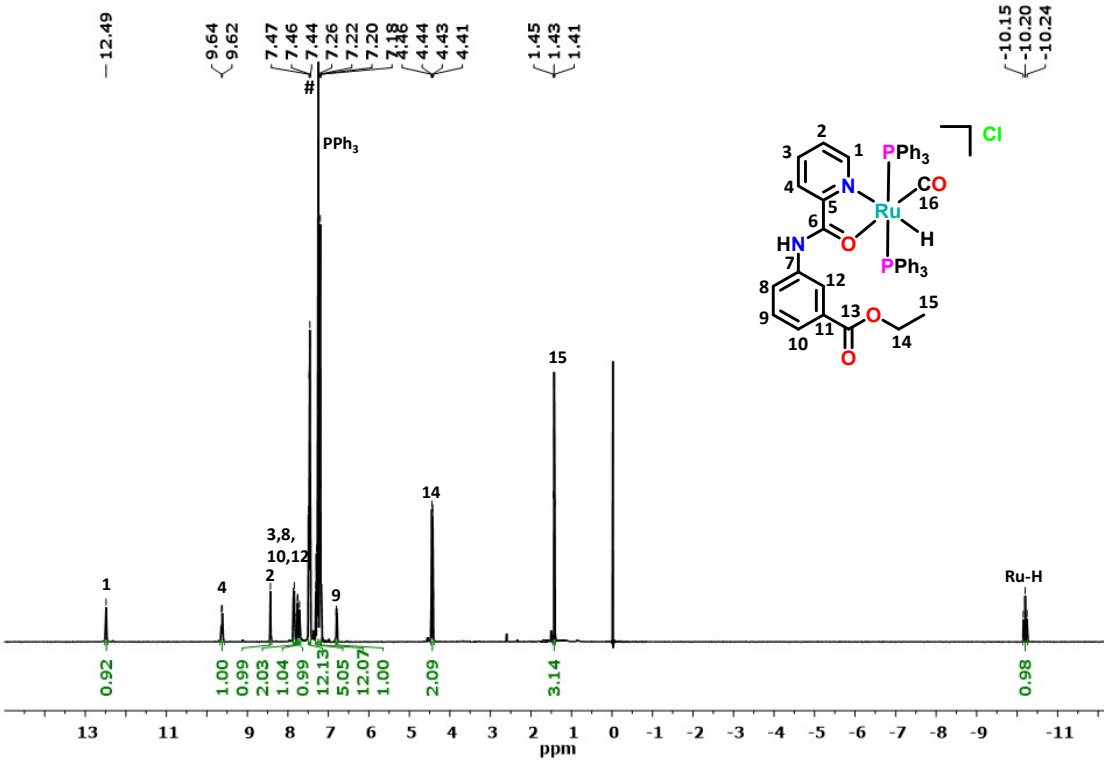

Figure S15. ^{1}H NMR spectrum of complex **3** in $CDCl_3$. # represents $CDCl_3$.

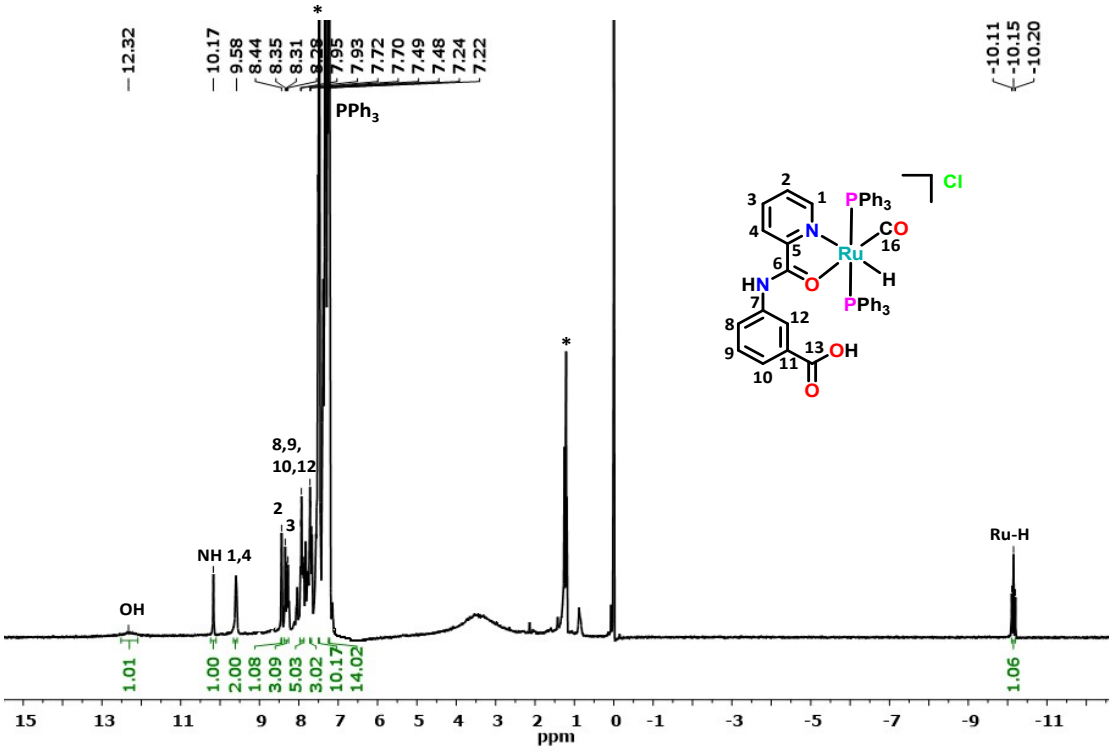

Figure S16. ^{1}H NMR spectrum of complex **4** in $CDCl_3$. * represents $CDCl_3$ /residual solvent/ H_2O peak.

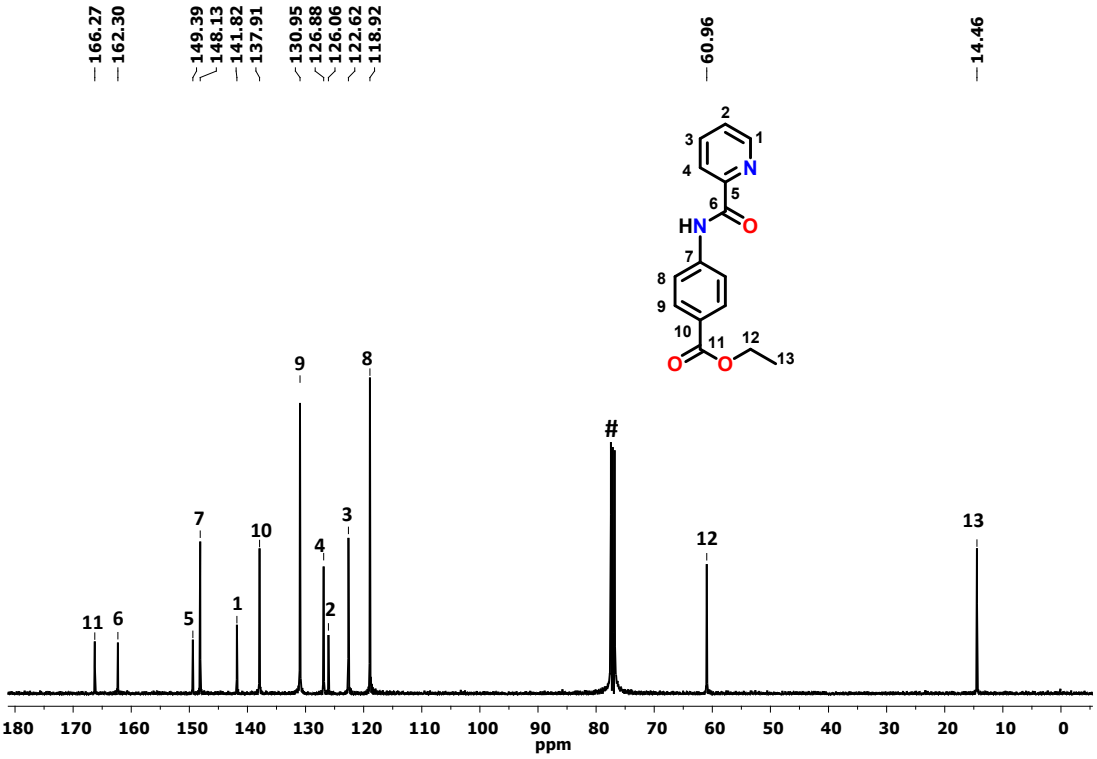

Figure S17. ^{13}C NMR spectrum of ligand H**L1** in $CDCl_3$. # Represent $CDCl_3$.

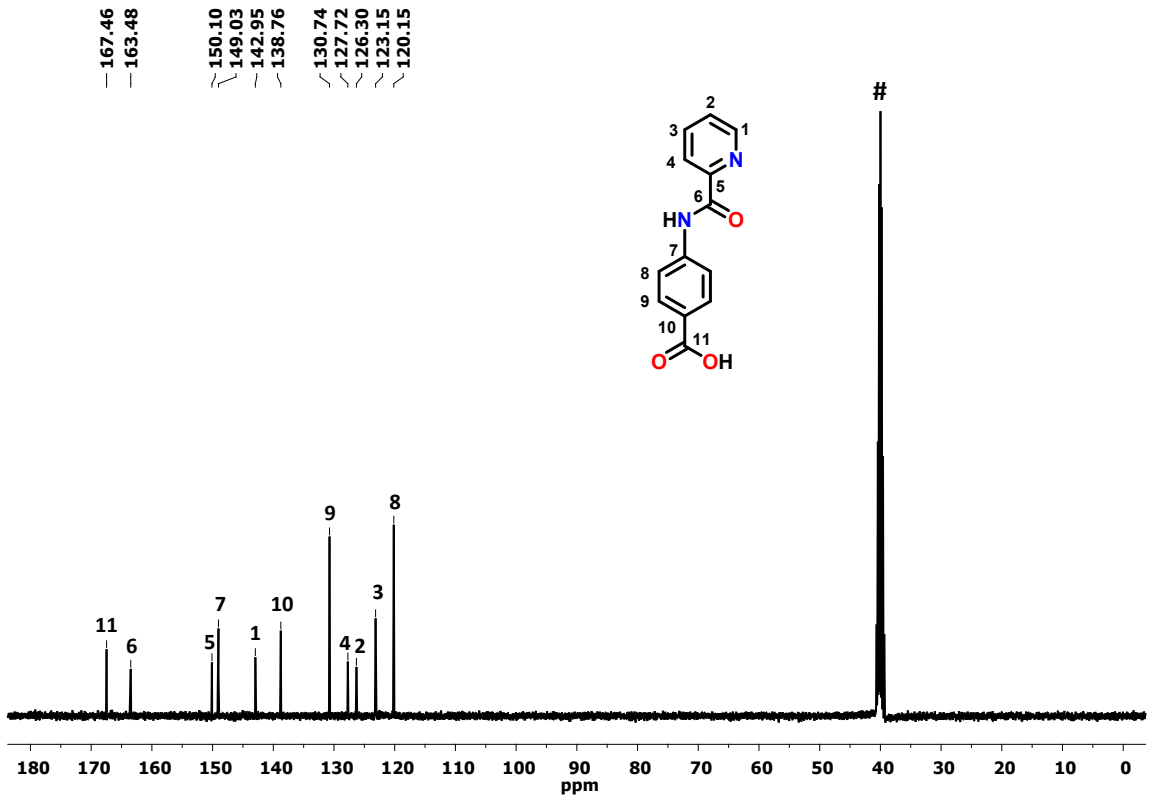

Figure S18. ^{13}C NMR spectrum of ligand H**L2** in DMSO-d_6. # Represent DMSO-d_6.

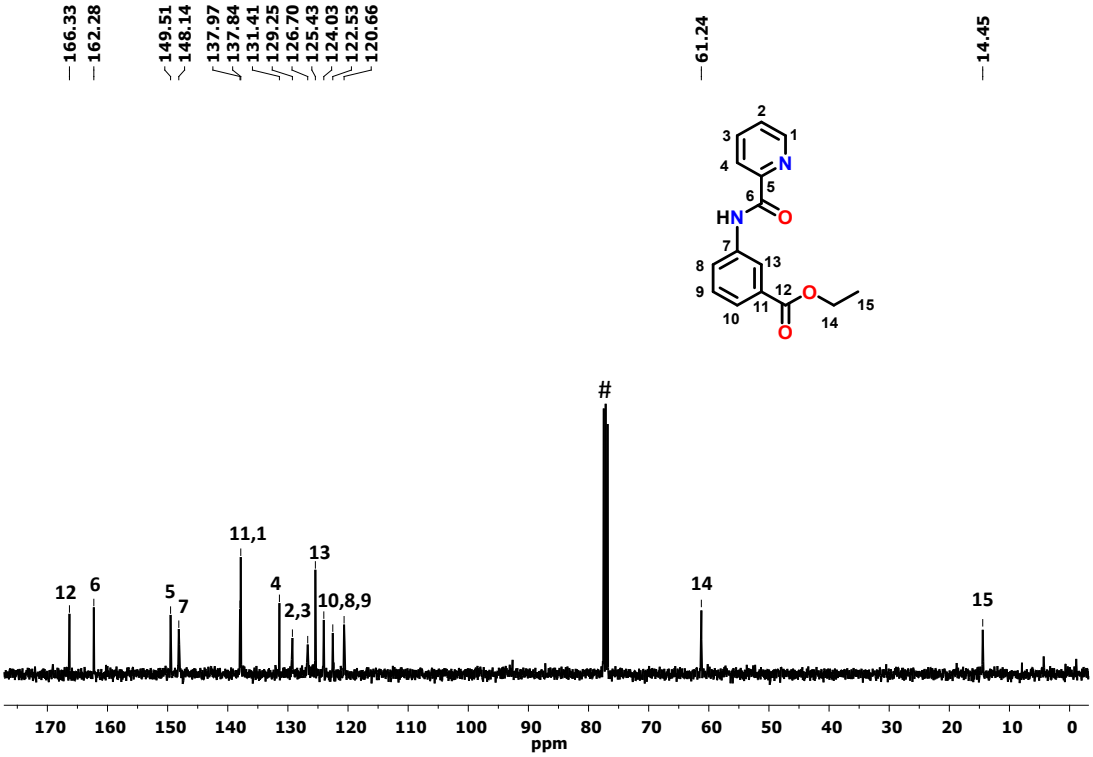

Figure S19. ^{13}C NMR spectrum of ligand H**L3** in $CDCl_3$. # Represents $CDCl_3$.

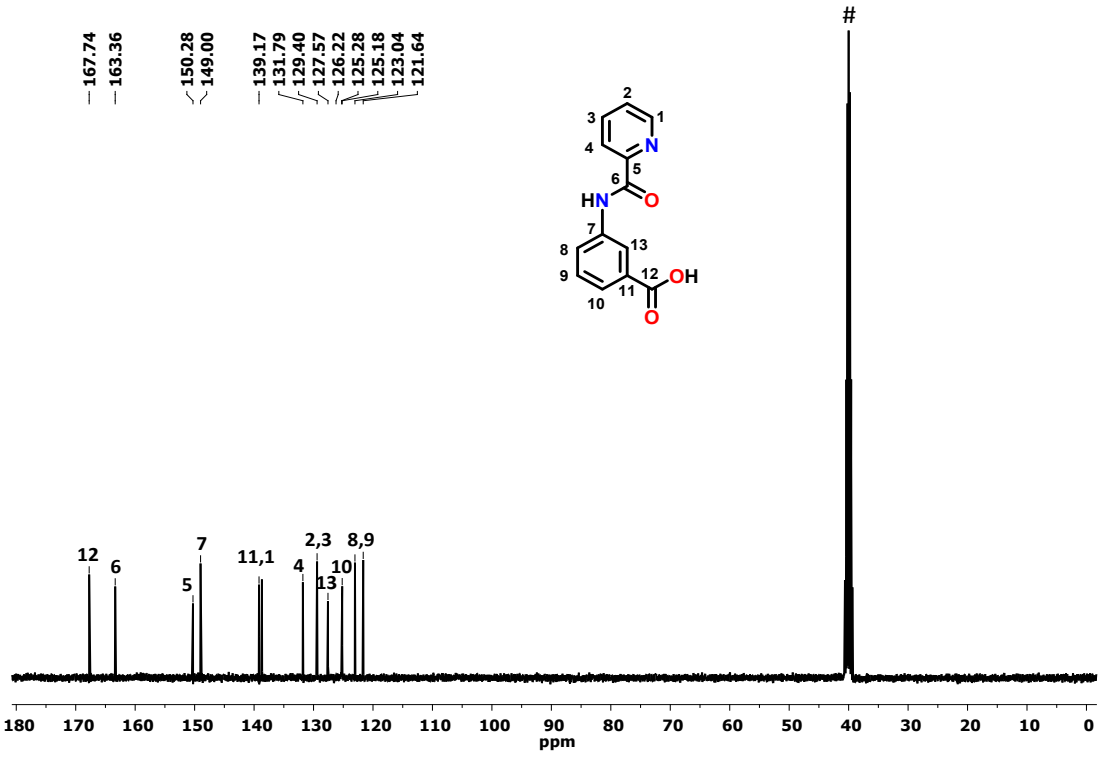

Figure S20. ^{13}C NMR spectrum of ligand H**L4** in DMSO-d_6. # Represents DMSO-d_6.

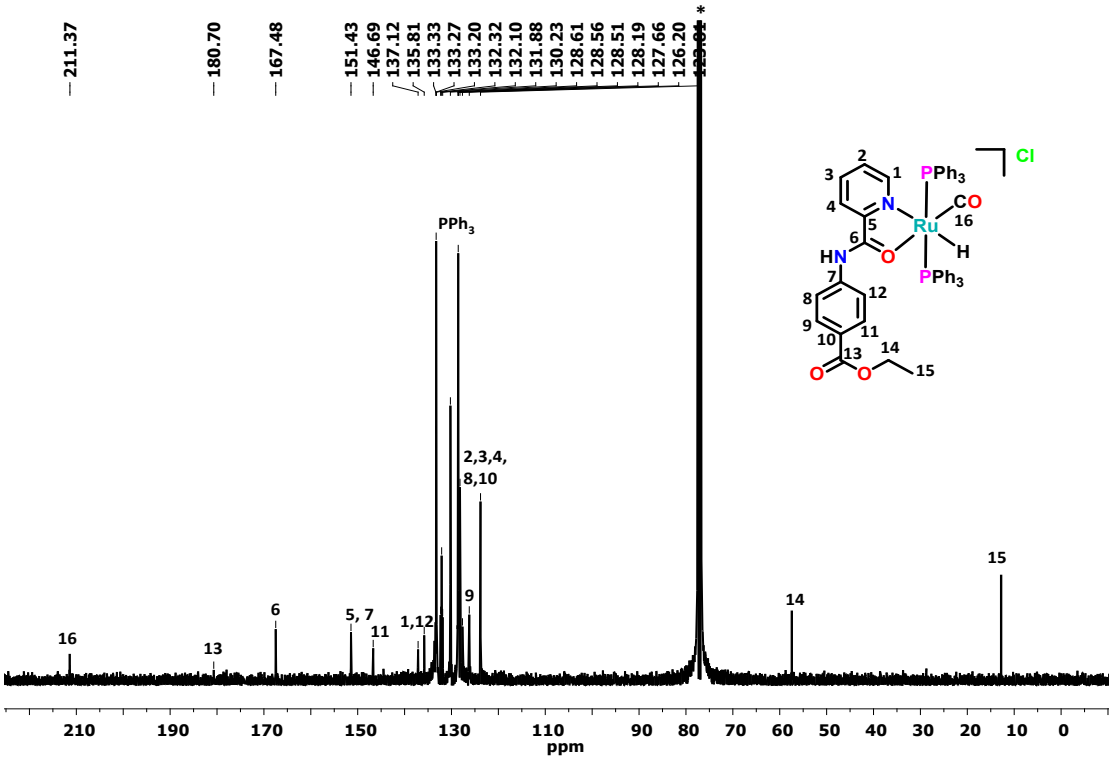

Figure S21. ^{13}C NMR spectrum of complex **1** in $CDCl_3$. * represents $CDCl_3$.

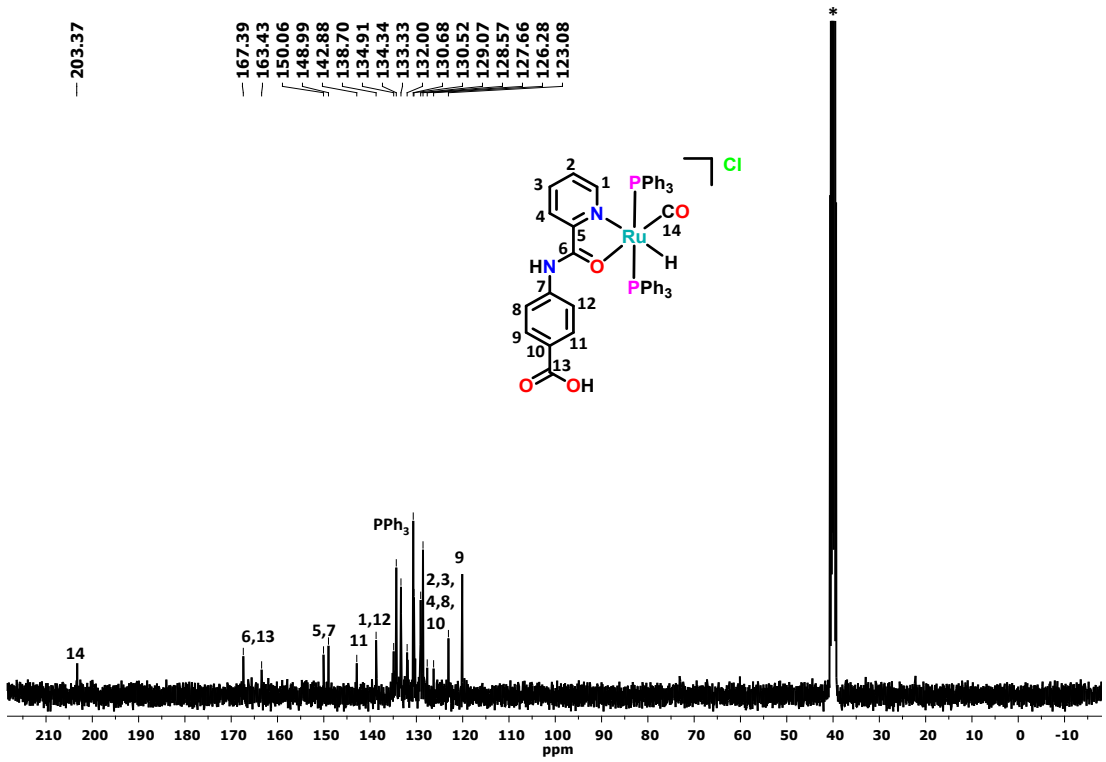

Figure S22. ^{13}C NMR spectrum of complex **2** in DMSO-d_6. * represents DMSO-d_6.

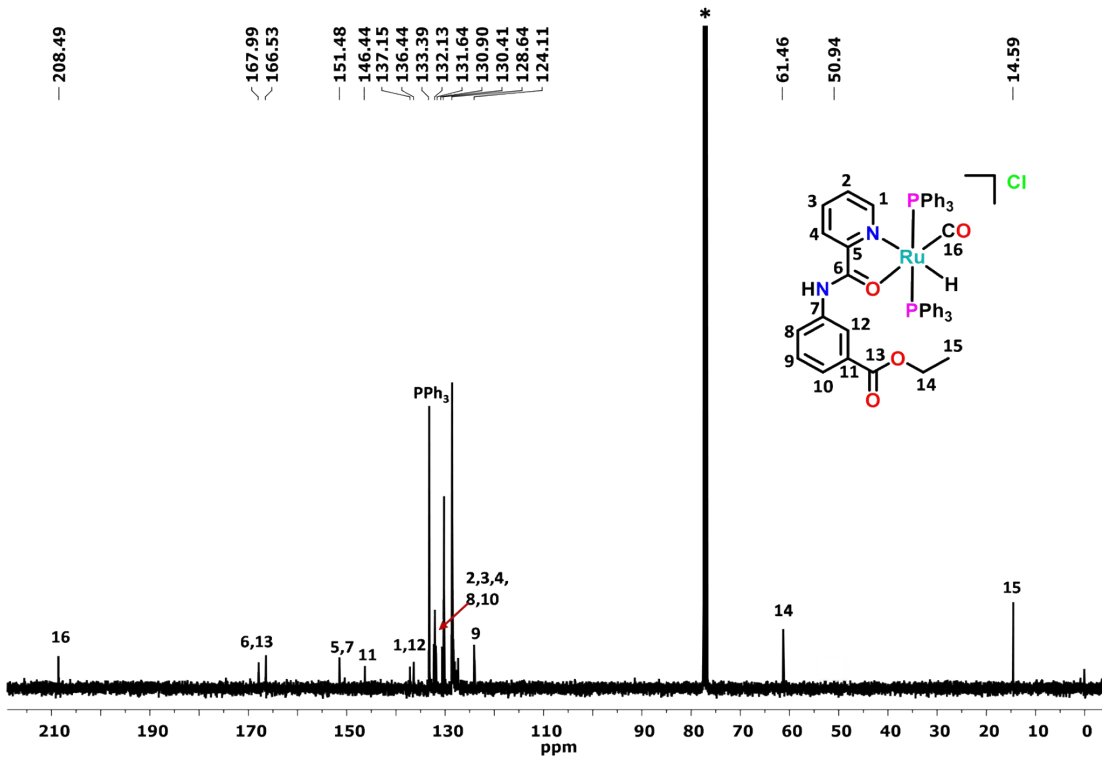

Figure S23. ^{13}C NMR spectrum of complex **3** in $CDCl_3$. * represents $CDCl_3$.

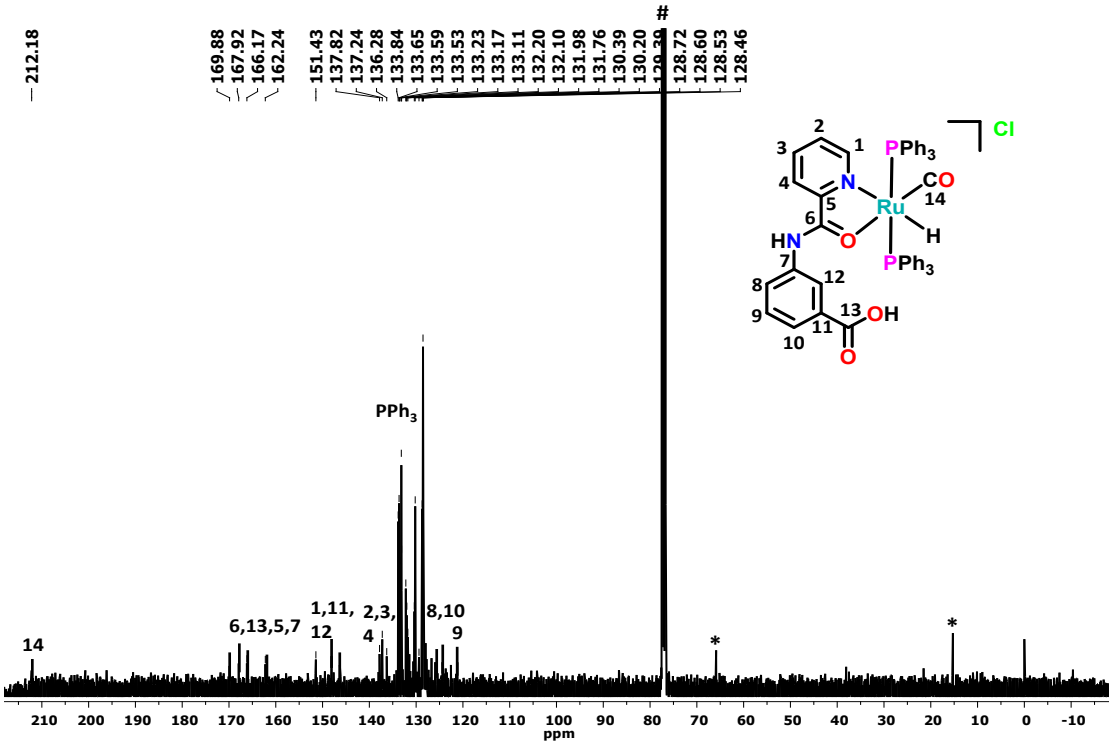

Figure S24. ^{13}C NMR spectrum of complex **4** in $CDCl_3$. # and * represent $CDCl_3$ and residual solvent, respectively.

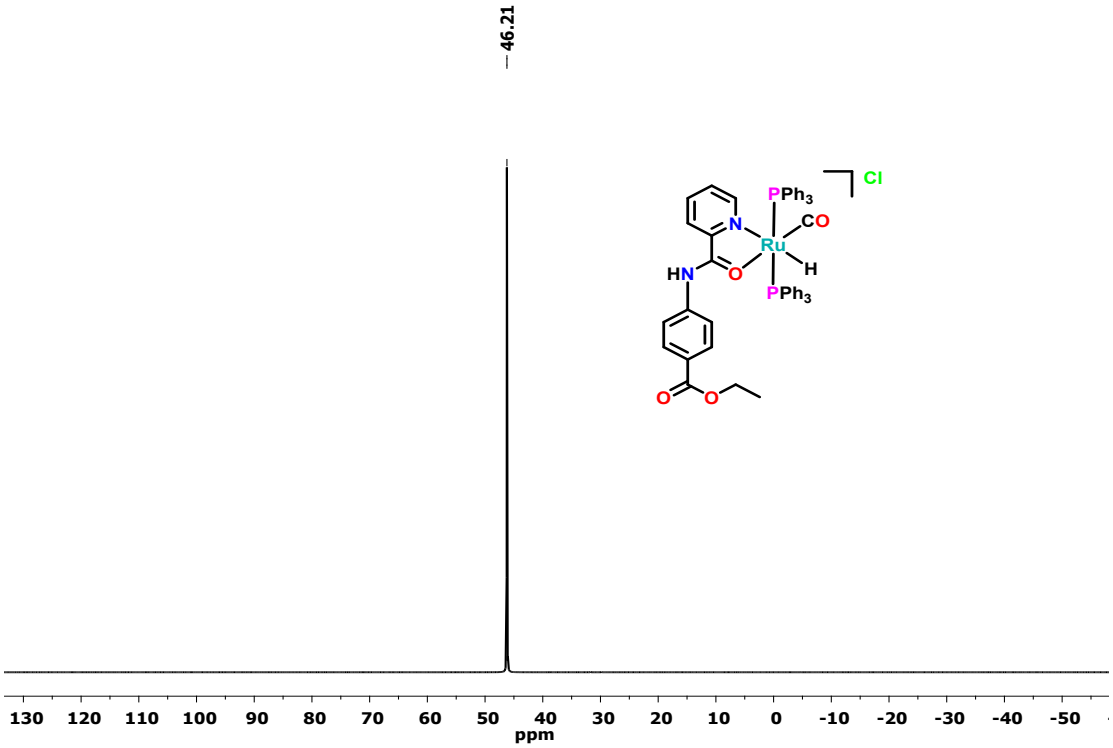

Figure S25. ^{31}P NMR spectrum of complex **1** in $CDCl_3$.

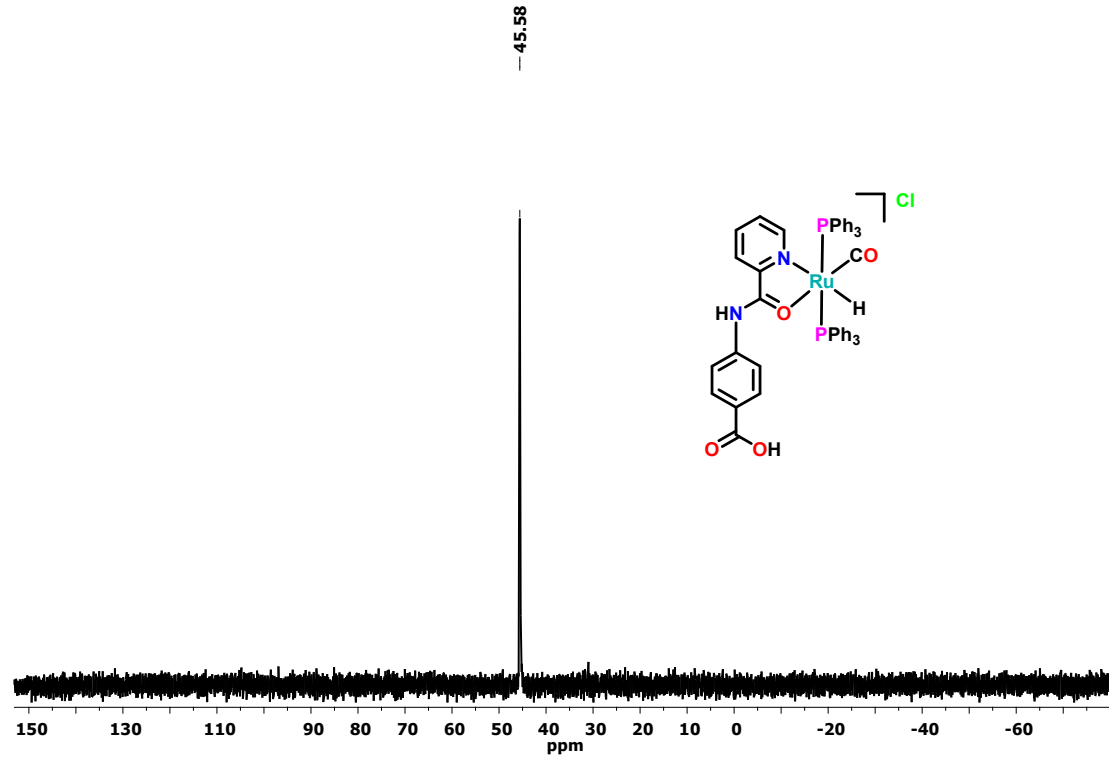

Figure S26. ^{31}P NMR spectrum of complex **2** in DMSO-d_6.

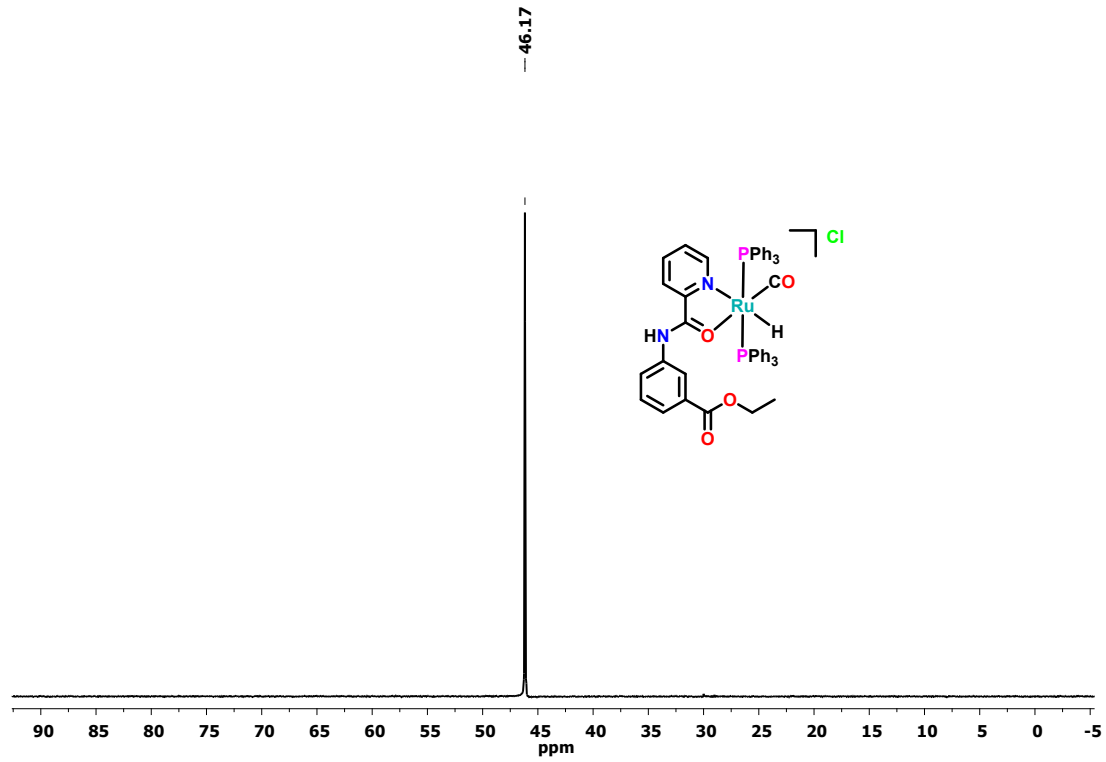

Figure S27. ^{31}P NMR spectrum of complex **3** in $CDCl_3$.

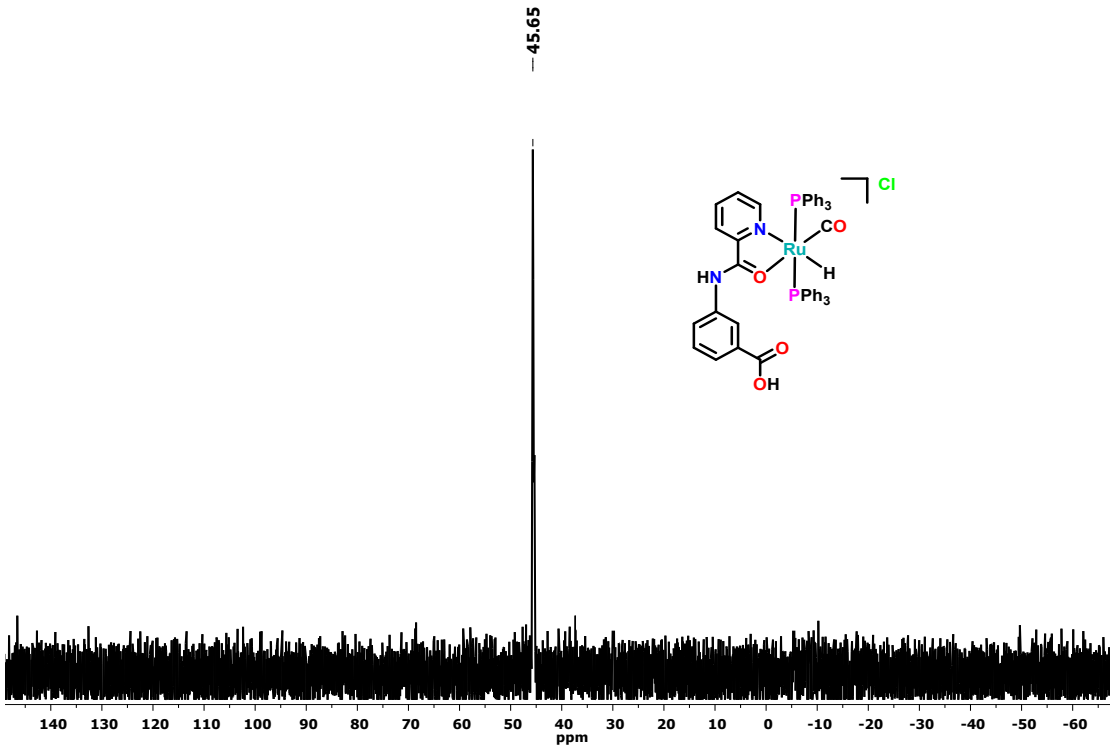

Figure S28. ^{31}P NMR spectrum of complex **4** in $CDCl_3$.

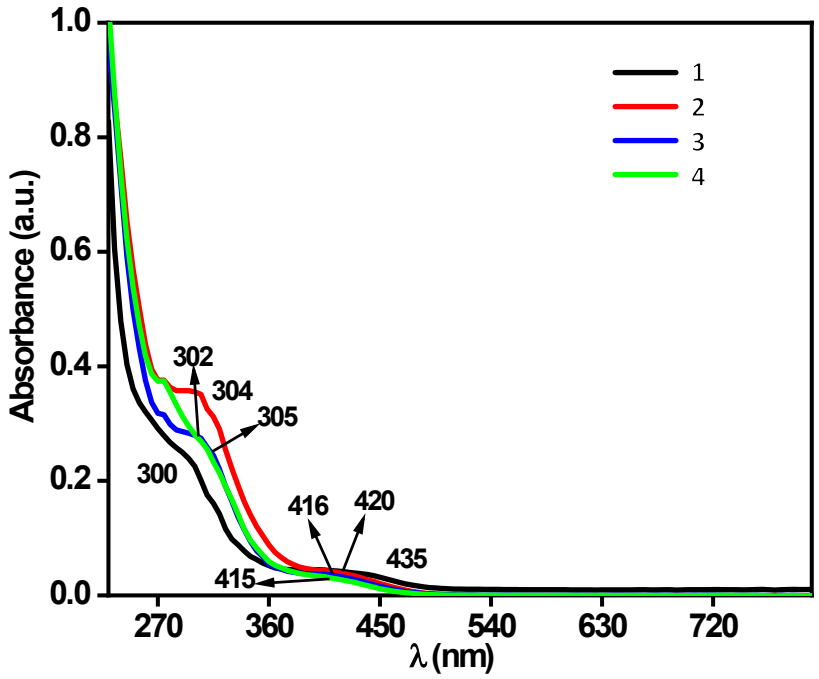

Figure S29. UV-Vis spectra of complexes **1-4** recorded in MeOH.

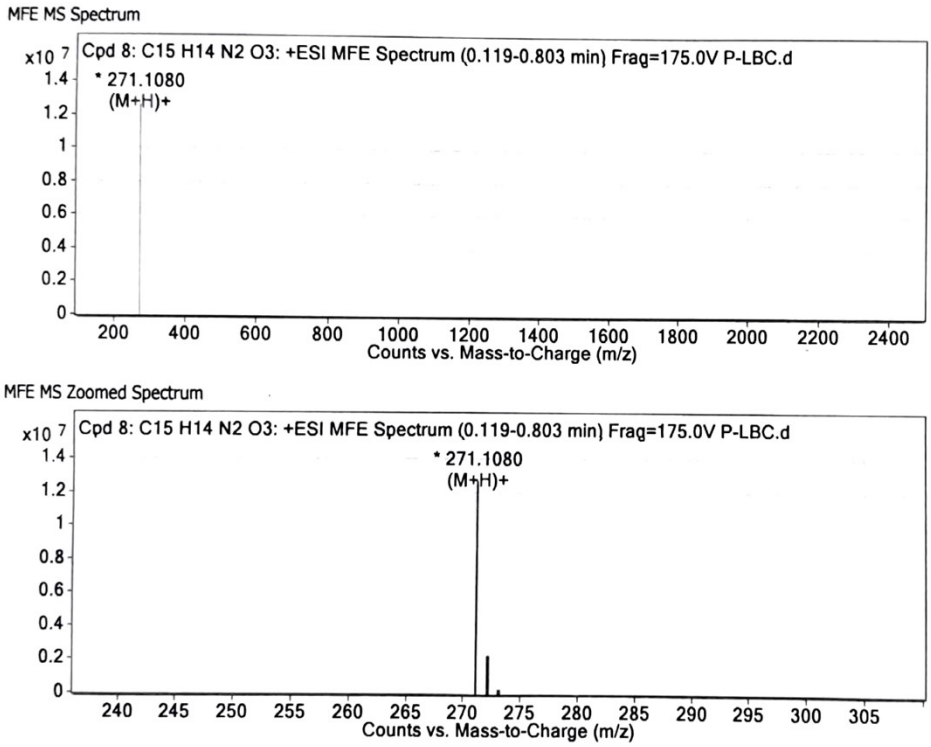

Figure S30. ESI$^+$-MS spectrum of ligand H**L1** in MeOH.

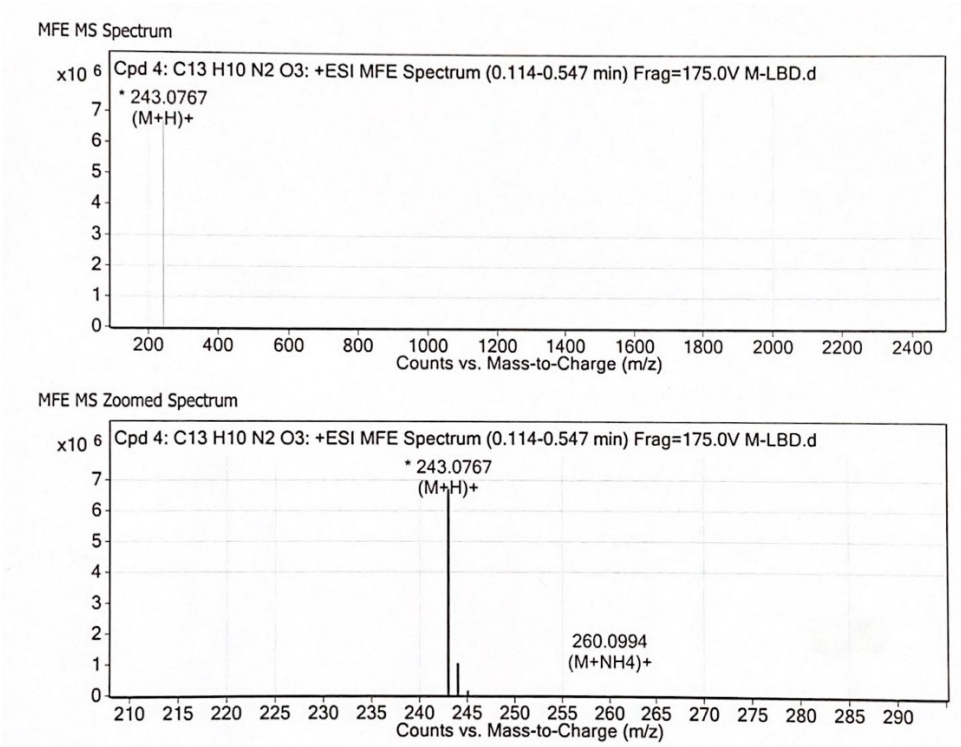

Figure S31. ESI$^+$-MS spectrum of ligand H**L2** in MeOH.

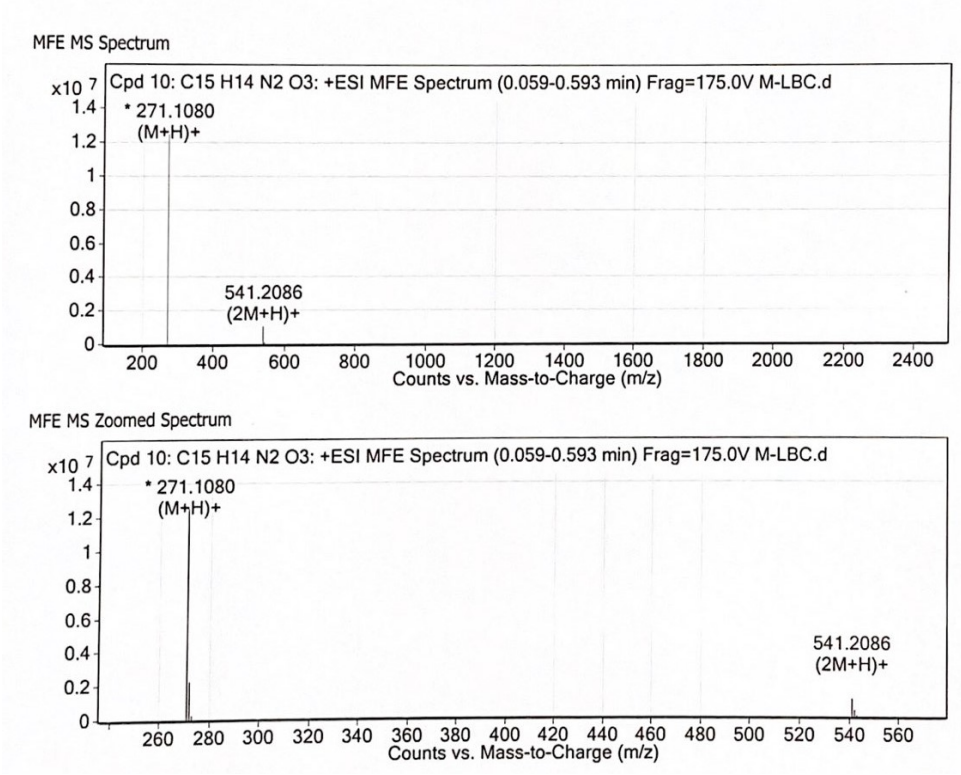

Figure S32. ESI$^+$-MS spectrum of ligand H**L3** in MeOH.

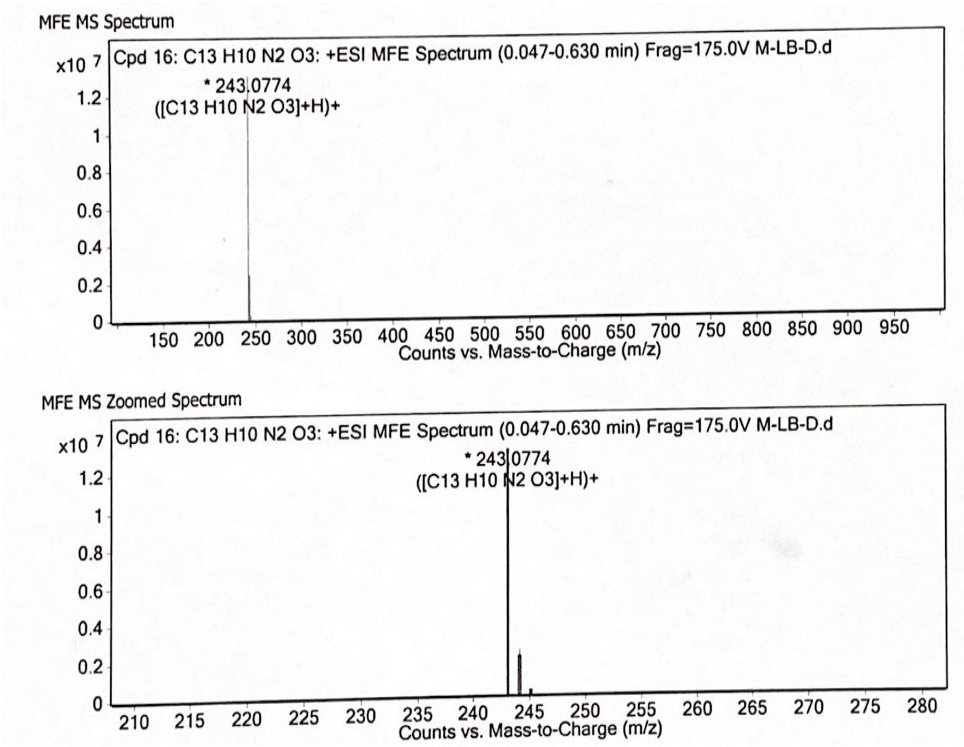

Figure S33. ESI$^+$-MS spectrum of ligand H**L4** in MeOH.

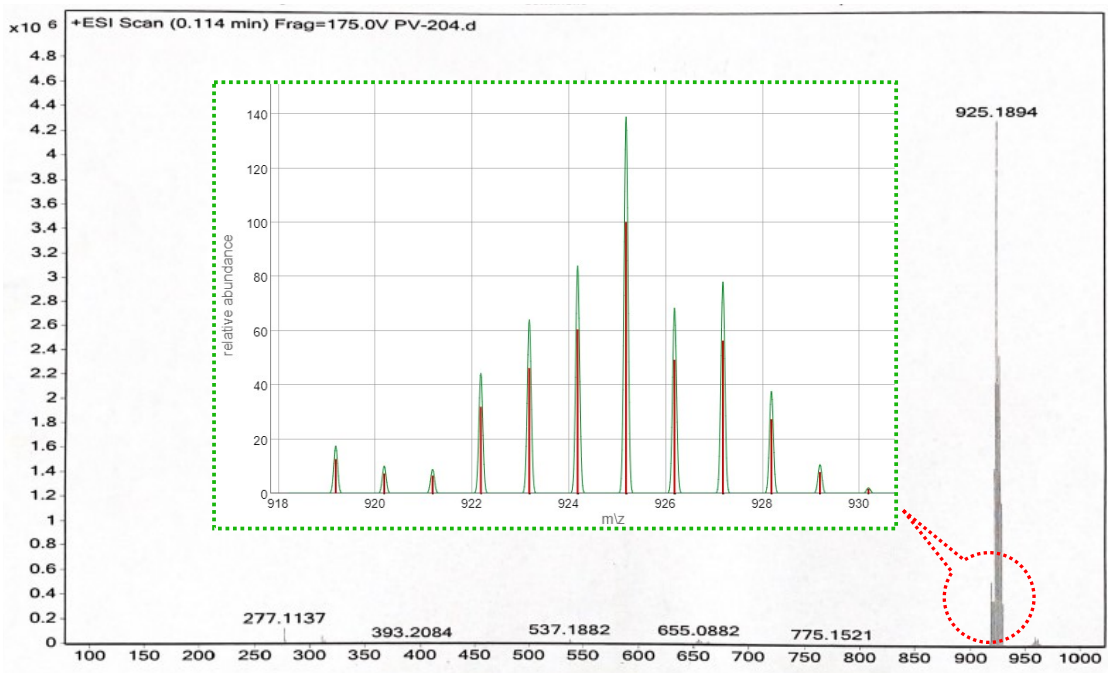

Figure S34. ESI$^+$-MS spectrum of complex **1** in MeOH. Inset: Experimental (green) and simulated (red) patterns for the molecular ion peak at *m/z* = 925.1894 $[M–Cl]^+$ for complex **1**.

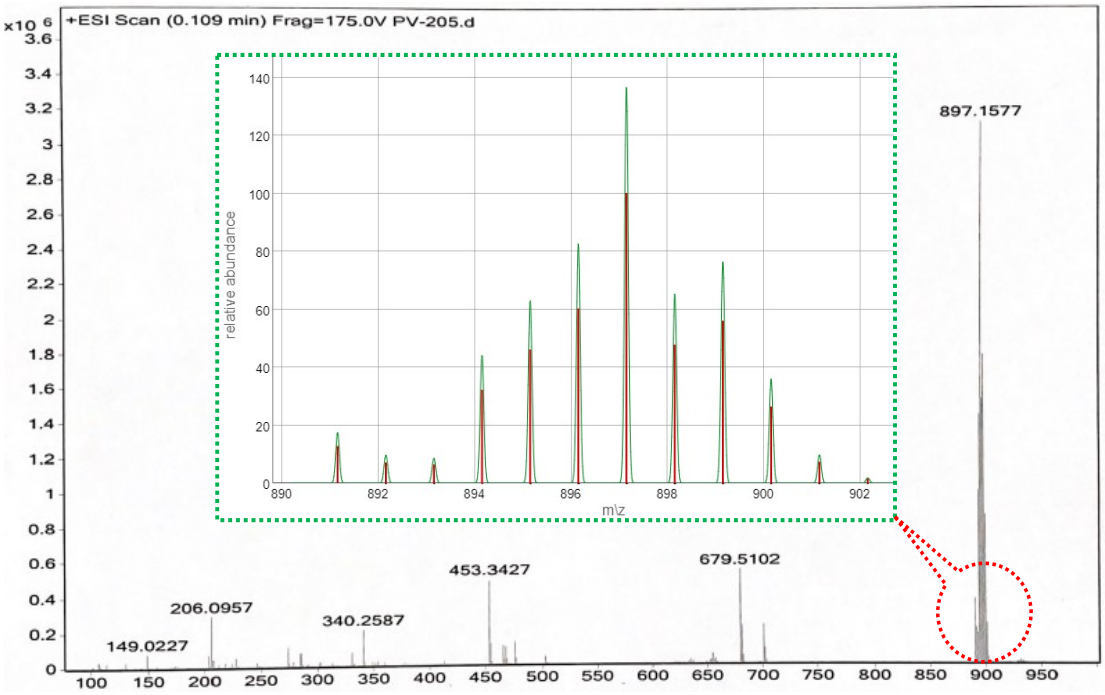

Figure S35. ESI$^+$-MS spectrum of complex **2** in MeOH. Inset: Experimental (green) and simulated (red) patterns for the molecular ion peak at *m/z* = 897.1577 $[M–Cl]^+$ for complex **2**.

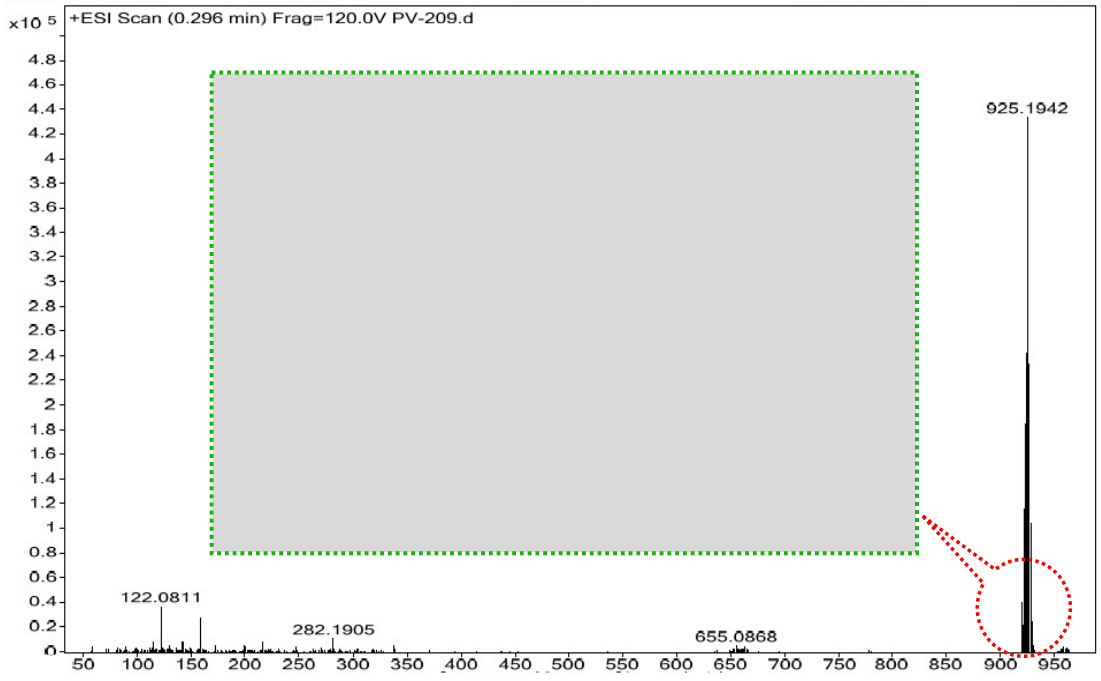

Figure S36. ESI$^+$-MS spectrum of complex **3** in MeOH. Inset: Experimental (green) and simulated (red) patterns for the molecular ion peak at *m/z* = 925.1942 $[M–Cl]^+$ for complex **3**.

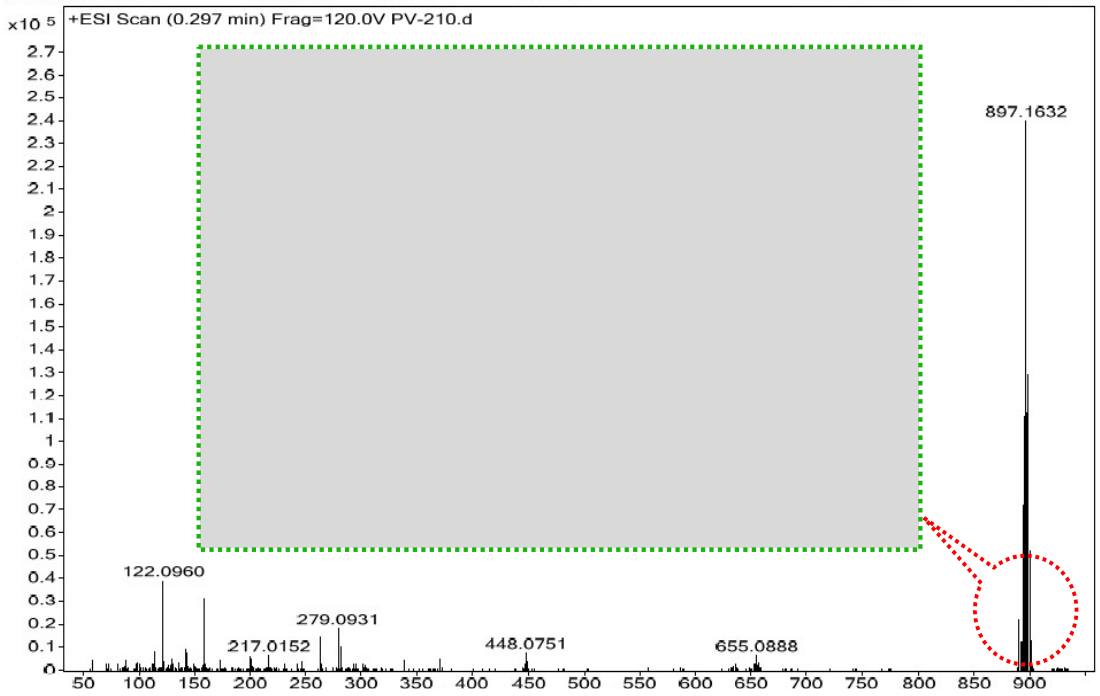

Figure S37. ESI$^+$-MS spectrum of complex **4** in MeOH. Inset: Experimental (green) and simulated (red) patterns for the molecular ion peak at *m/z* = 897.1632 $[M–Cl]^+$ for complex **4**.

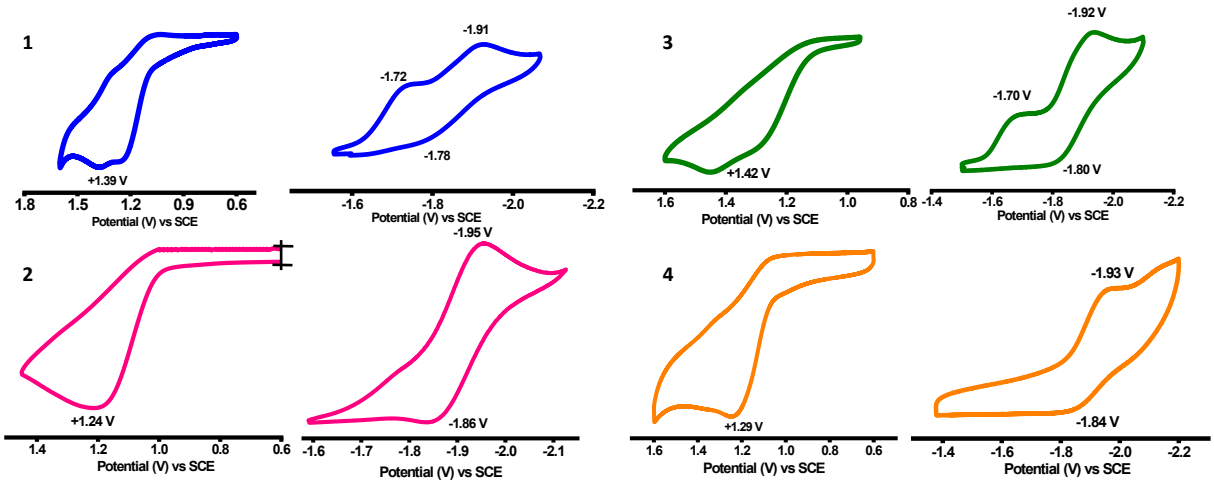

Figure S38. Cyclic voltammograms for complexes **1 – 4**. Conditions: solvent, DMF; complex, ca. 1 mM; supporting electrolyte, TBAP, ca. 100 mM; working electrode, glassy carbon; reference electrode, Ag/Ag$^+$; auxiliary electrode, Pt wire; scan rate, 100 mV/s.

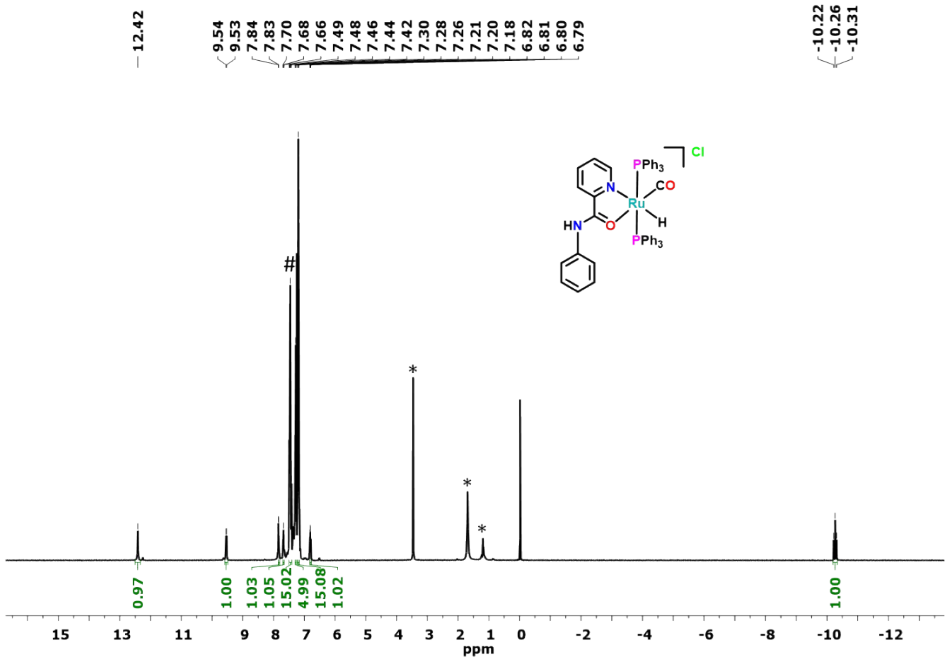

Figure S39. ^{1}H NMR spectrum of complex **5** in $CDCl_3$. # and * represent $CDCl_3$ and residual solvent/ H_2O peak, respectively.

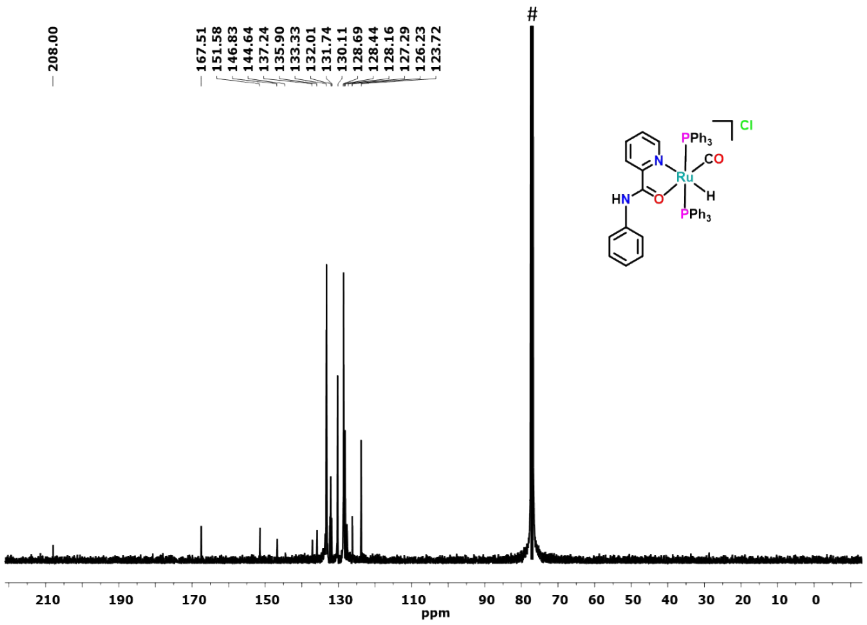

Figure S40. ^{13}C NMR spectrum of complex **5** in $CDCl_3$. # represents $CDCl_3$.

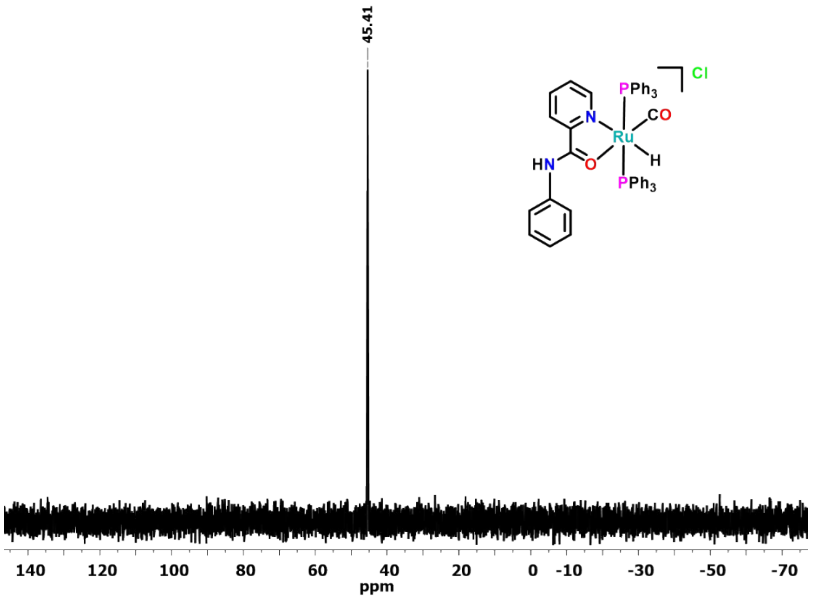

Figure 41. ^{31}P NMR spectrum of complex **5** in $CDCl_3$.

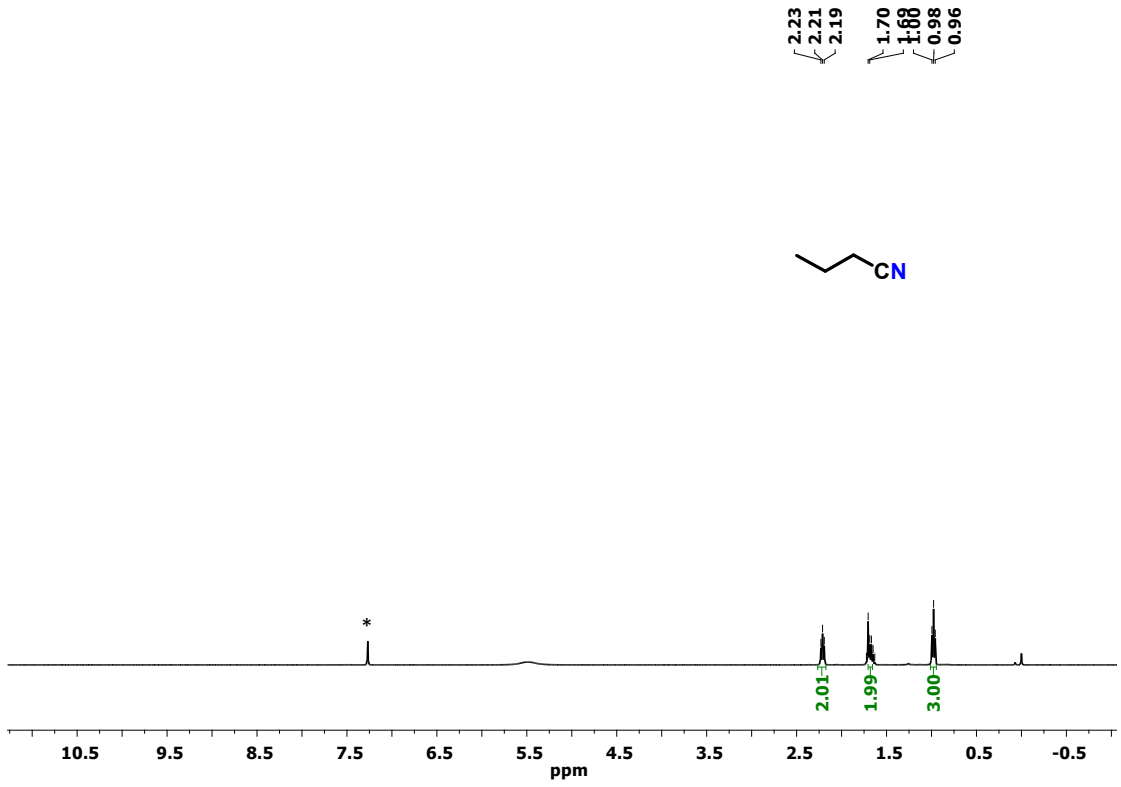

Figure S42. ^{1}H NMR spectrum of butyronitrile (table 2, entry 1) in $CDCl_3$. * represents $CDCl_3$ peak.

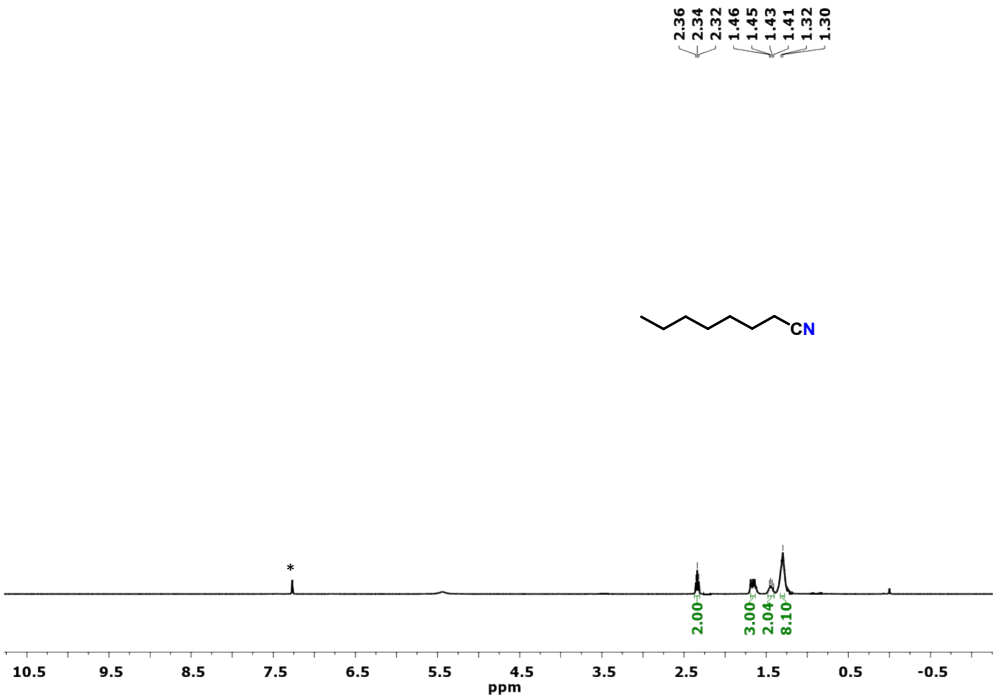

Figure S43. ^{1}H NMR spectrum of octanenitrile (table 2, entry 2) in $CDCl_3$. * represents $CDCl_3$ peak.

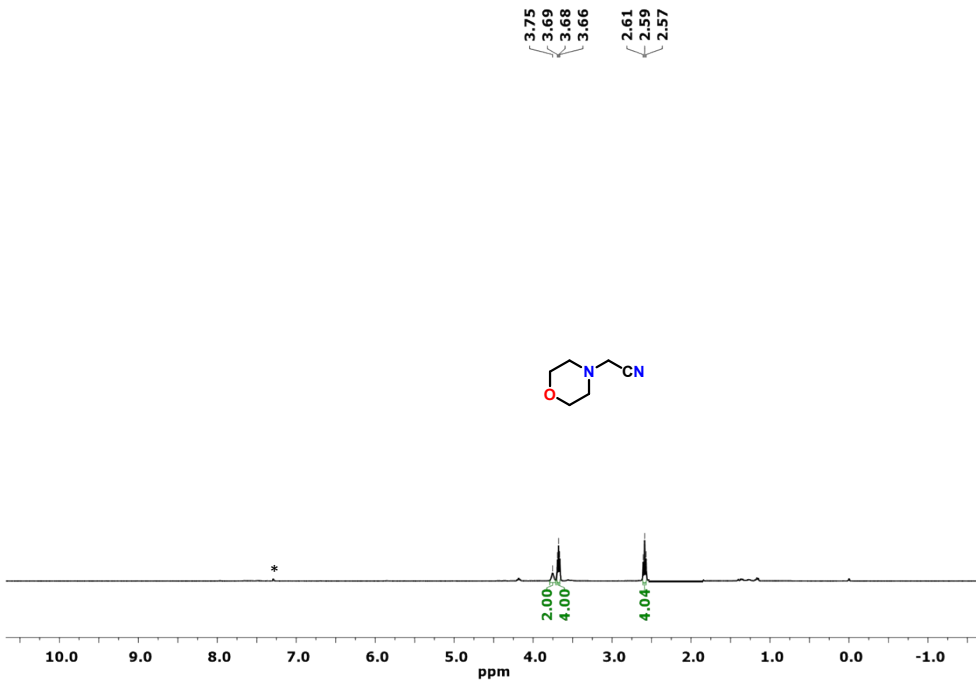

Figure S44. ^{1}H NMR spectrum of 2-morpholinoacetonitrile (table 2, entry 3) in $CDCl_3$. * represents $CDCl_3$ peak.

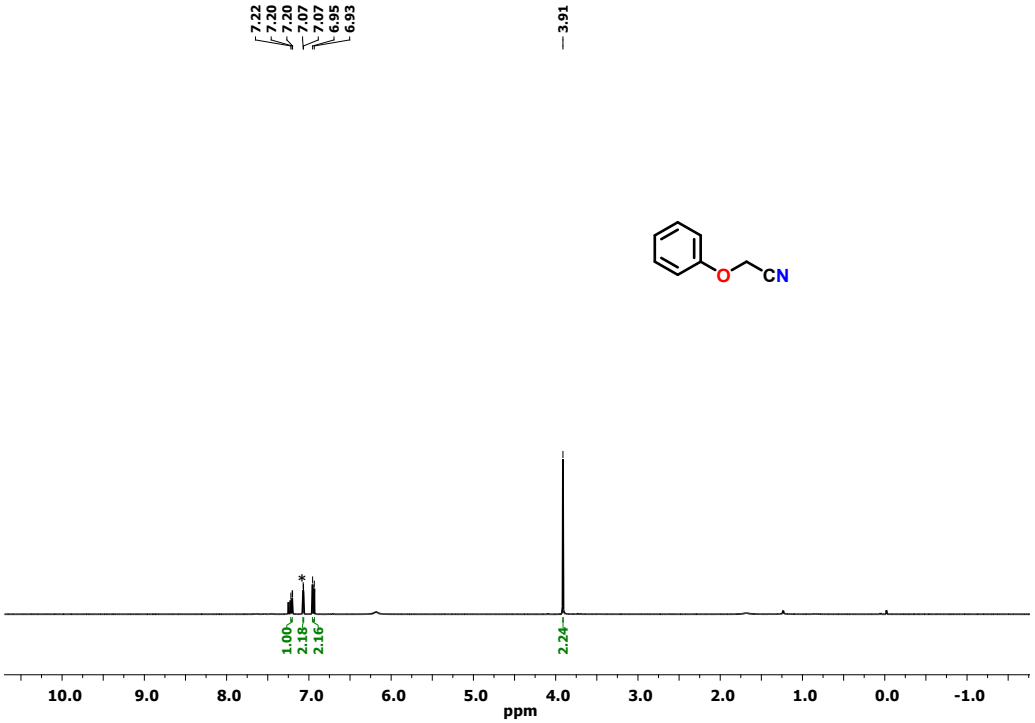

Figure S45. ^{1}H NMR spectrum of 2-phenoxyacetonitrile (table 2, entry 4) in $CDCl_3$. * represents $CDCl_3$ peak.

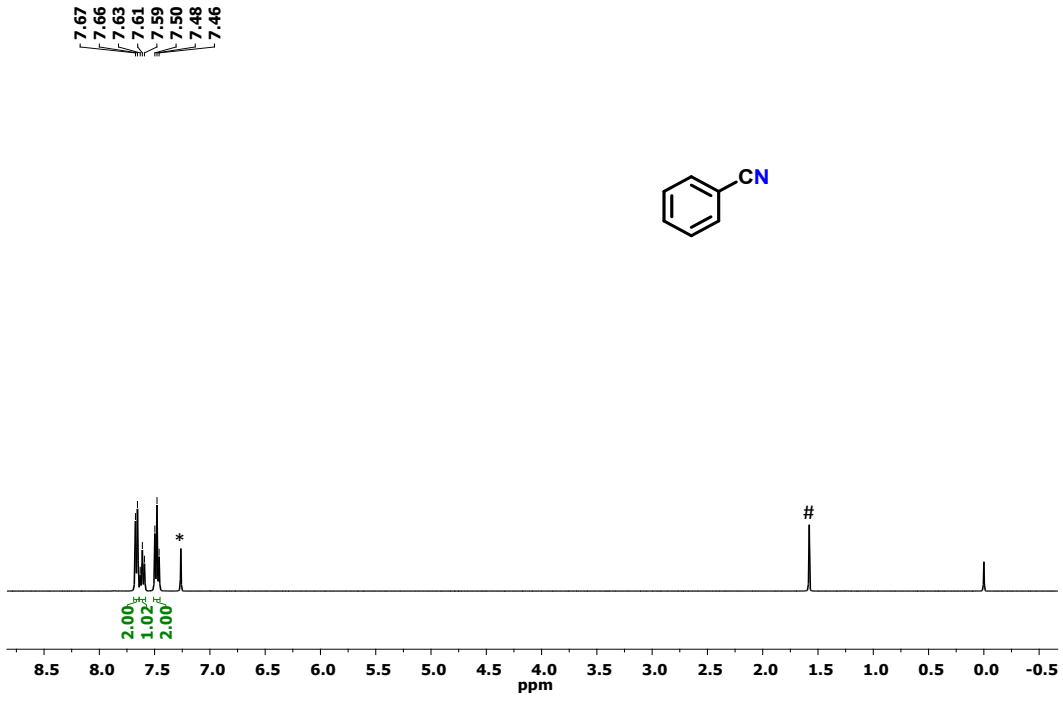

Figure S46. ^{1}H NMR spectrum of benzonitrile (table 3, entry 1) in $CDCl_3$. * and # represent $CDCl_3$ and H_2O peaks, respectively.

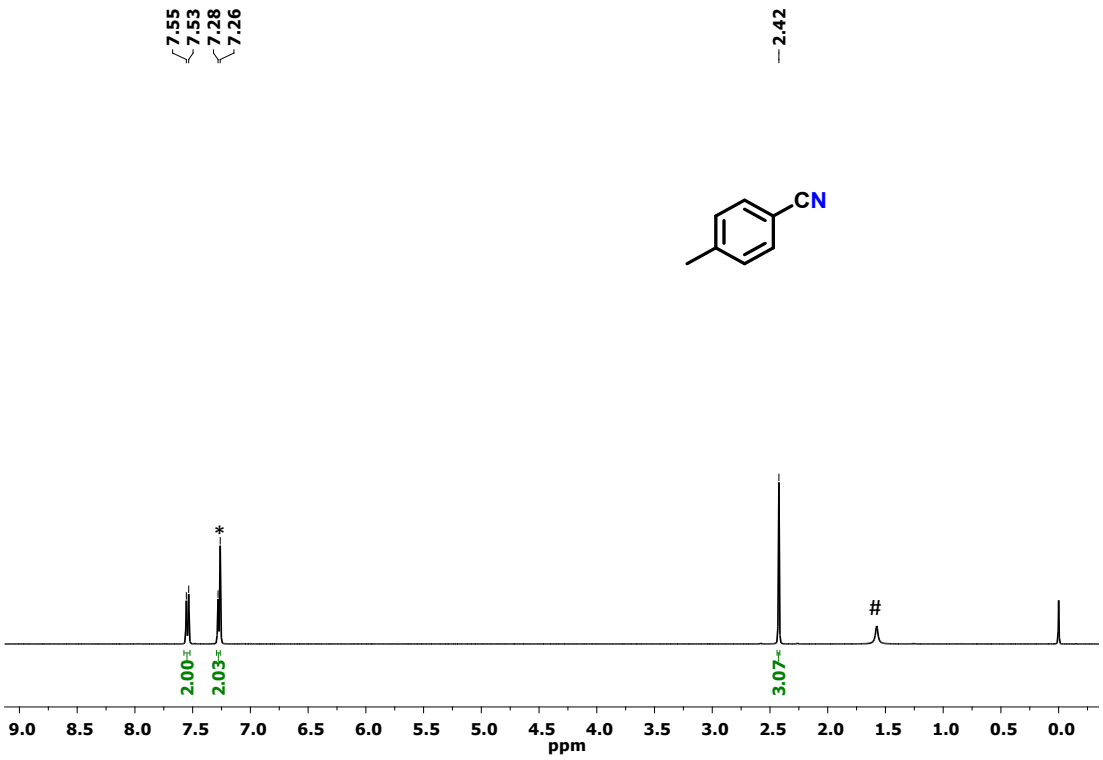

Figure S47. ^{1}H NMR spectrum of 4-methylbenzonitrile (table 3, entry 2) in $CDCl_3$. * and # represent $CDCl_3$ and H_2O peaks, respectively.

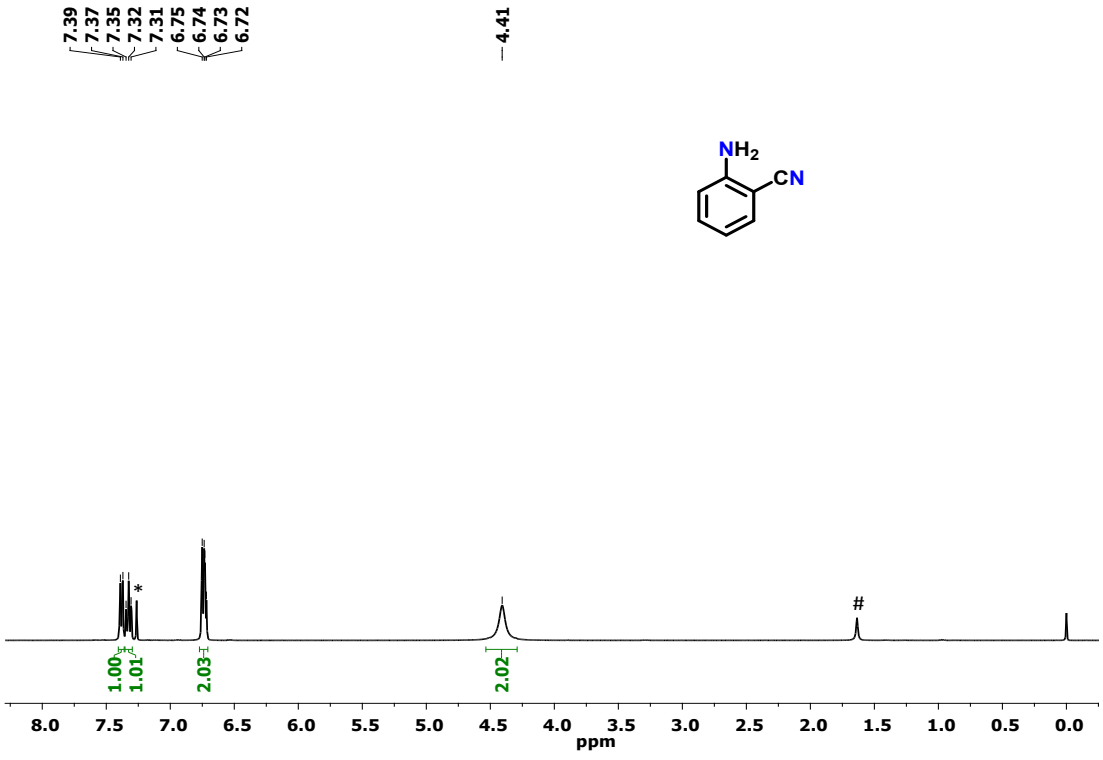

Figure S48. ^{1}H NMR spectrum of 2-aminobenzonitrile (table 3, entry 3) in $CDCl_3$. * and # represent $CDCl_3$ and H_2O peaks, respectively.

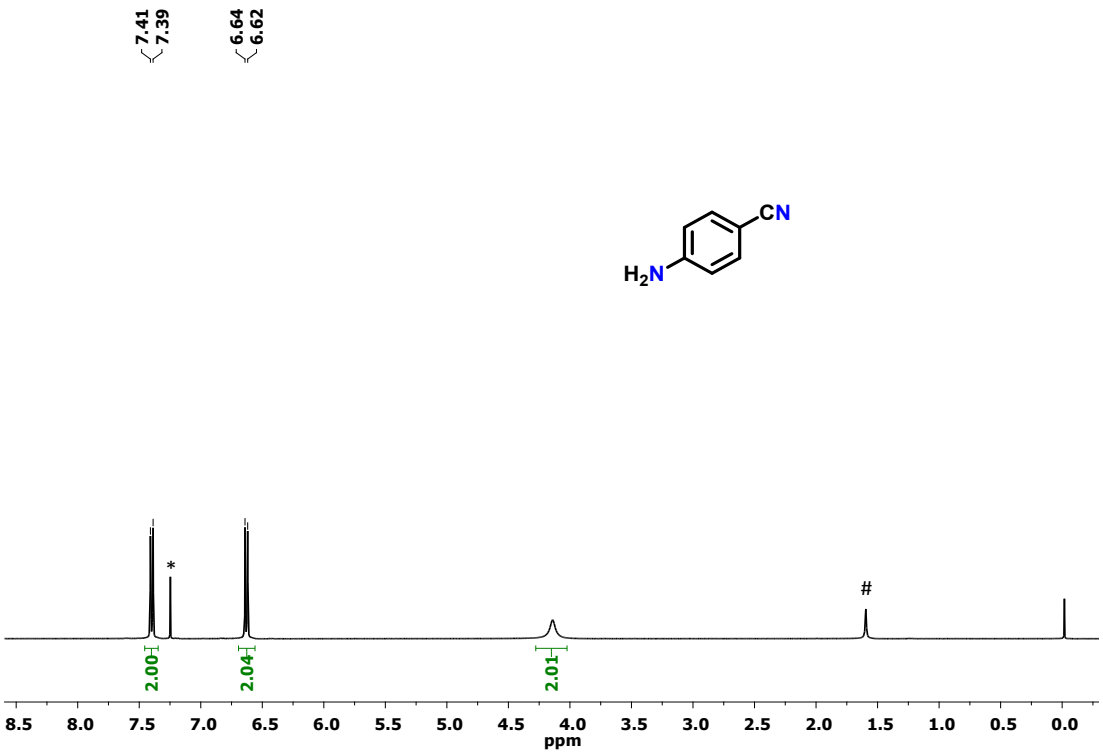

Figure S49. ^{1}H NMR spectrum of 4-aminobenzonitrile (table 3, entry 4) in $CDCl_3$. * and # represent $CDCl_3$ and H_2O peaks, respectively.

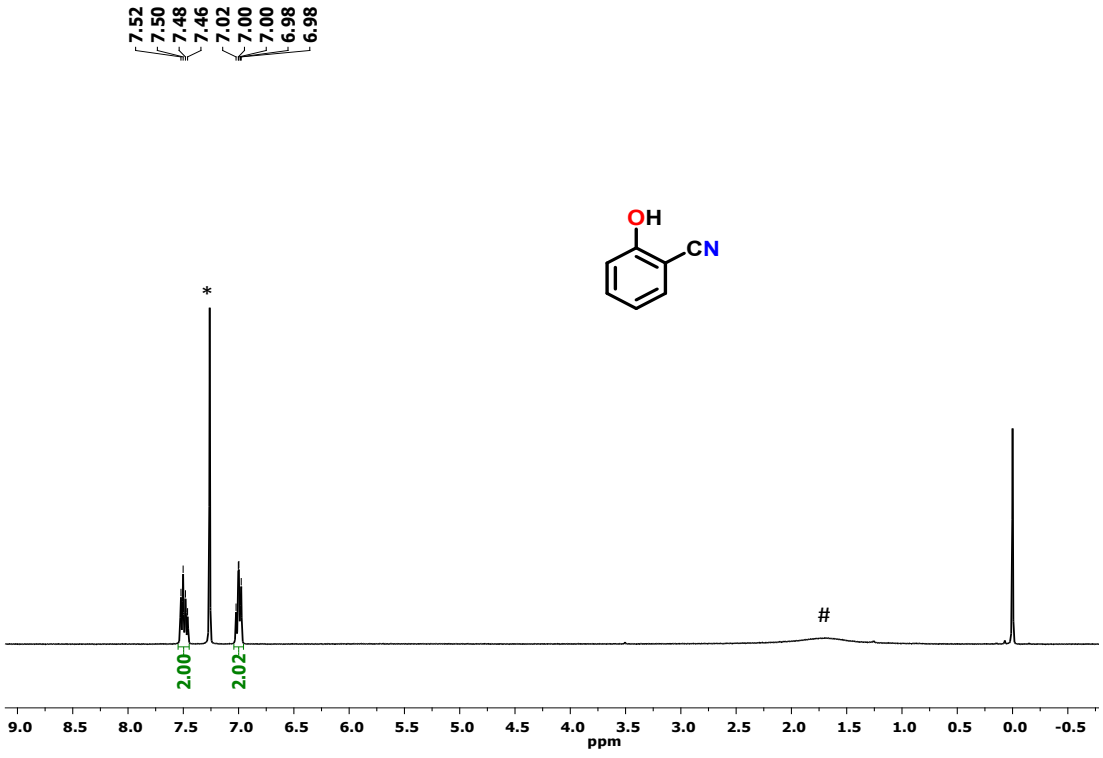

Figure S50. ^{1}H NMR spectrum of 2-hydroxybenzonitrile (table 3, entry 5) in $CDCl_3$. * and # represent $CDCl_3$ and H_2O peaks, respectively.

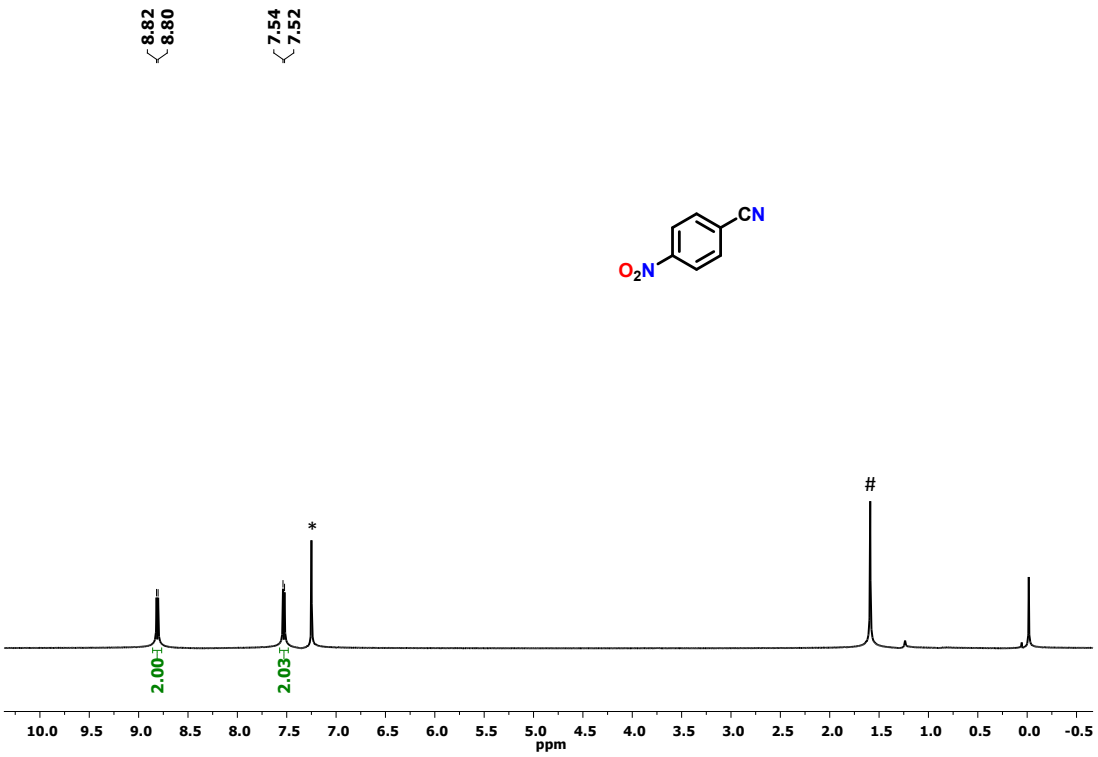

Figure S51. ^{1}H NMR spectrum of 4-nitrobenzonitrile (table 3, entry 6) in $CDCl_3$. * and # represent $CDCl_3$ and H_2O peaks, respectively.

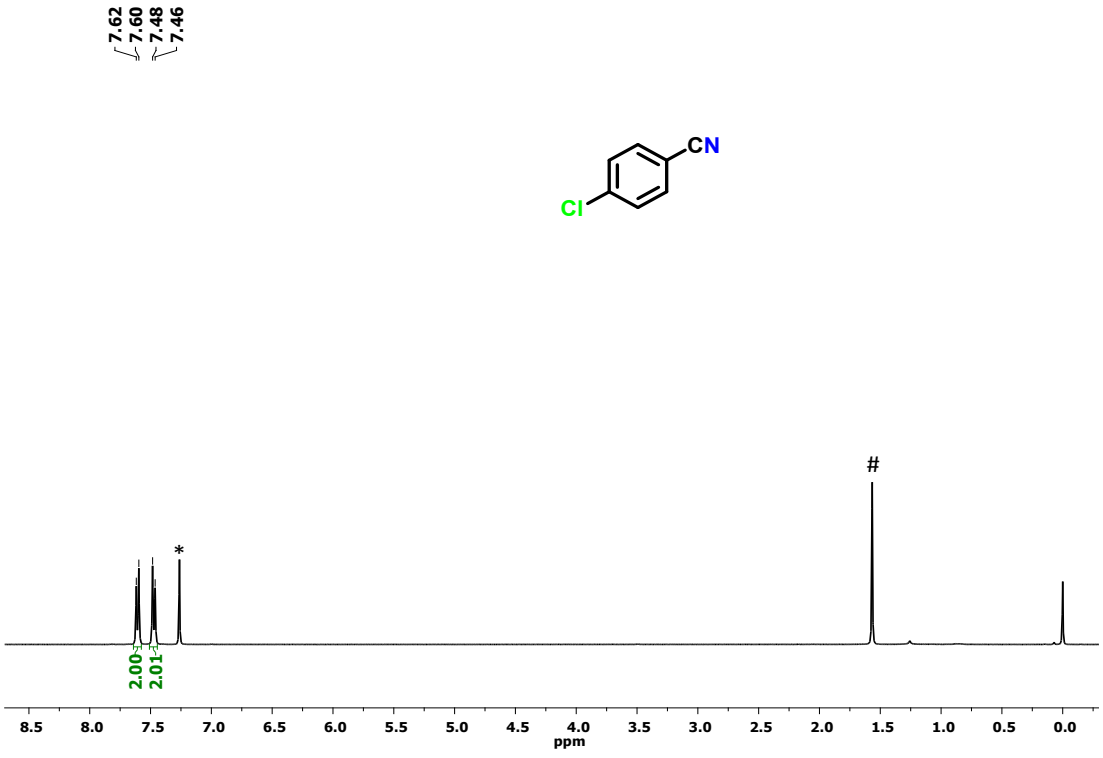

Figure S52. ^{1}H NMR spectrum of 4-chlorobenzonitrile (table 3, entry 7) in $CDCl_3$. * and # represent $CDCl_3$ and H_2O peaks, respectively.

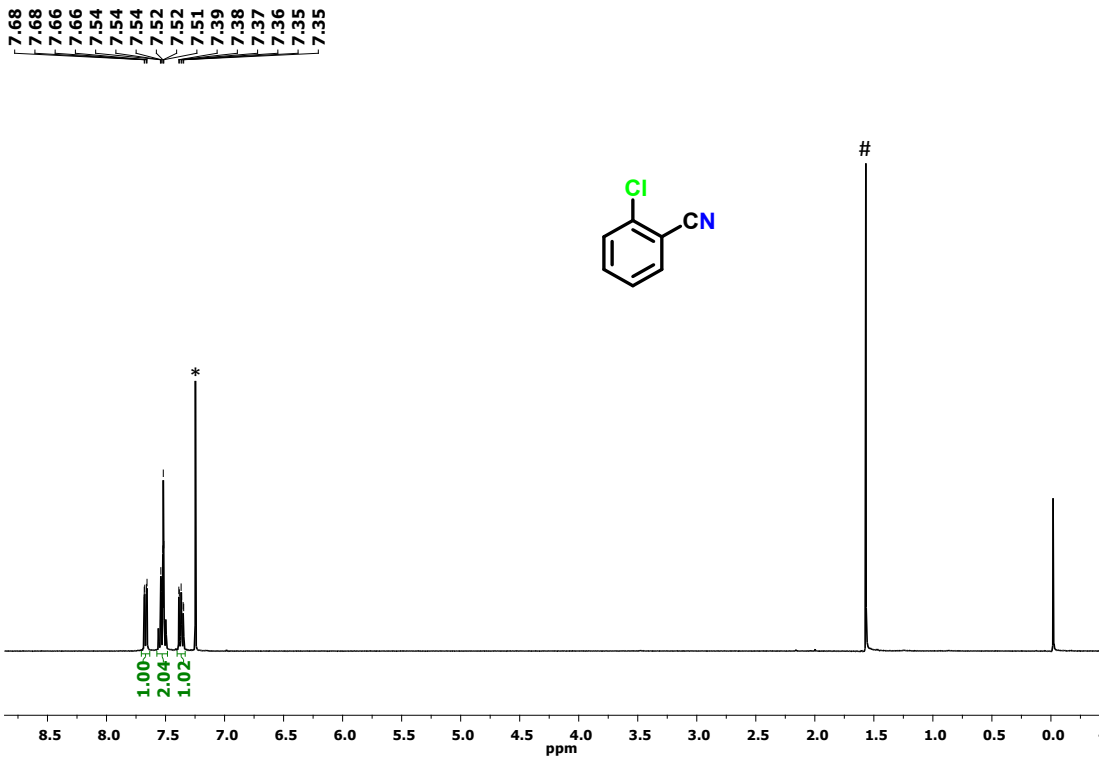

Figure S53. ^{1}H NMR spectrum of 2-chlorobenzonitrile (table 3, entry 8) in $CDCl_3$. * and # represent $CDCl_3$ and H_2O peaks, respectively.

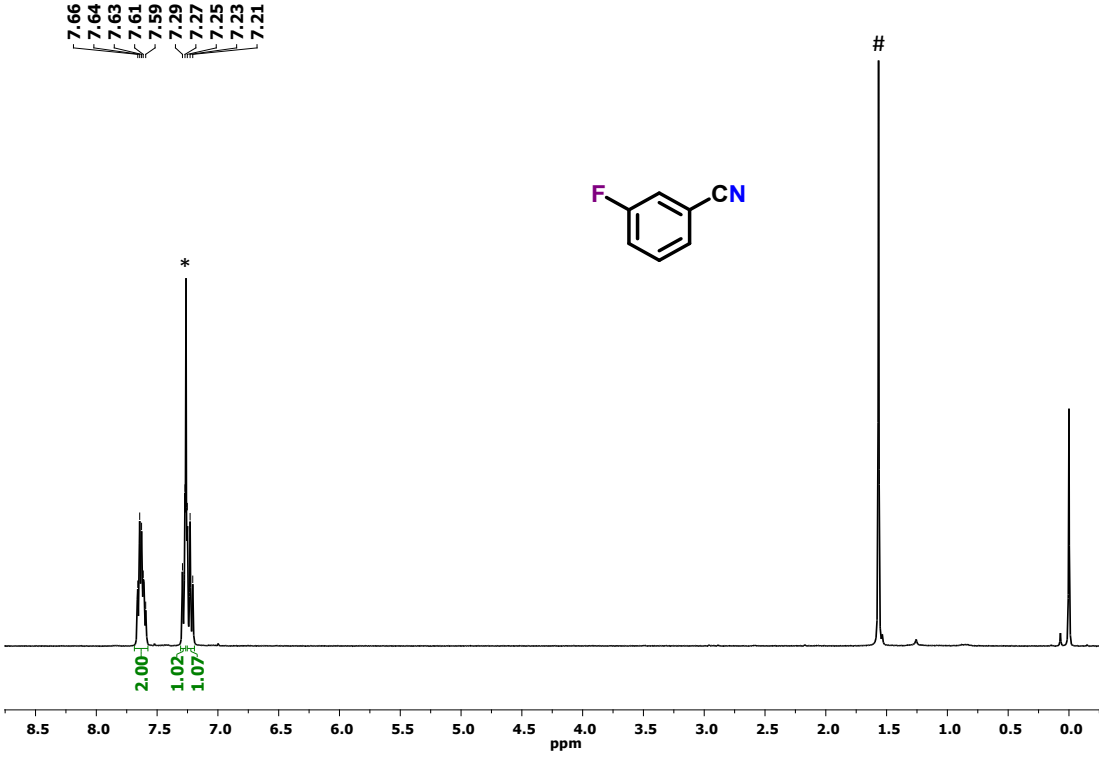

Figure S54. ^{1}H NMR spectrum of 3-fluorobenzonitrile (table 3, entry 9) in $CDCl_3$. * and # represent $CDCl_3$ and H_2O peaks, respectively.

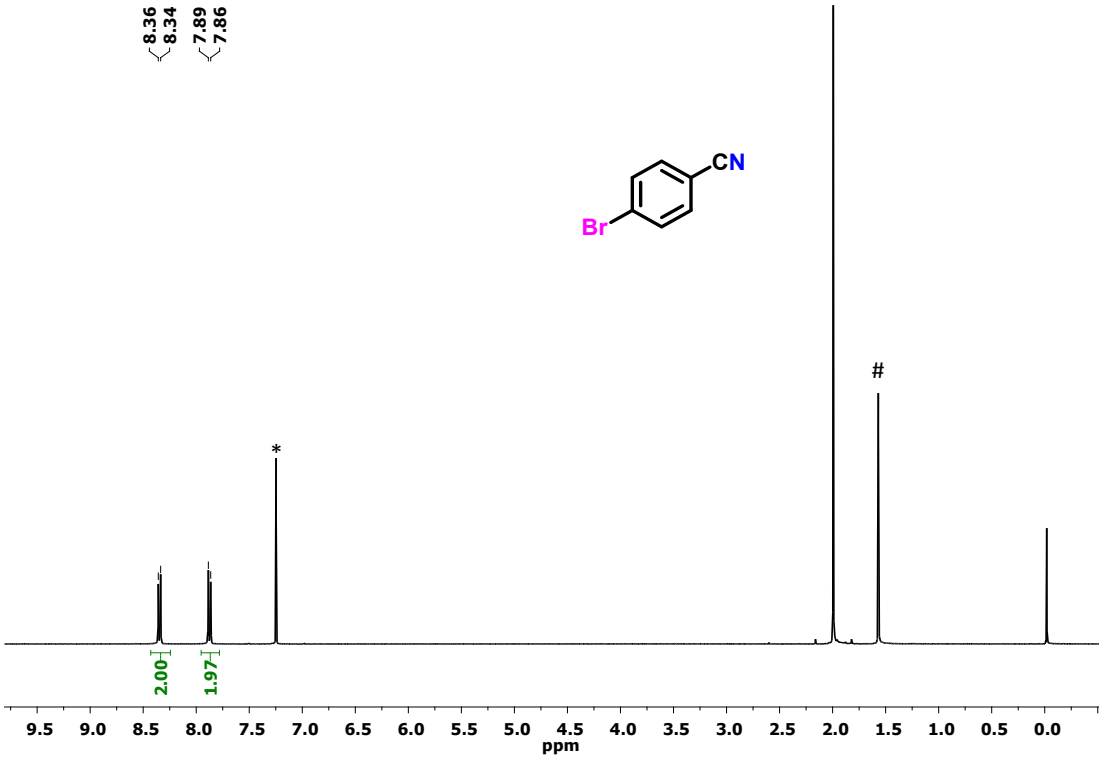

Figure S55. ^{1}H NMR spectrum of 4-bromobenzonitrile (table 3, entry 10) in $CDCl_3$. * and # represent $CDCl_3$ and H_2O peaks, respectively.

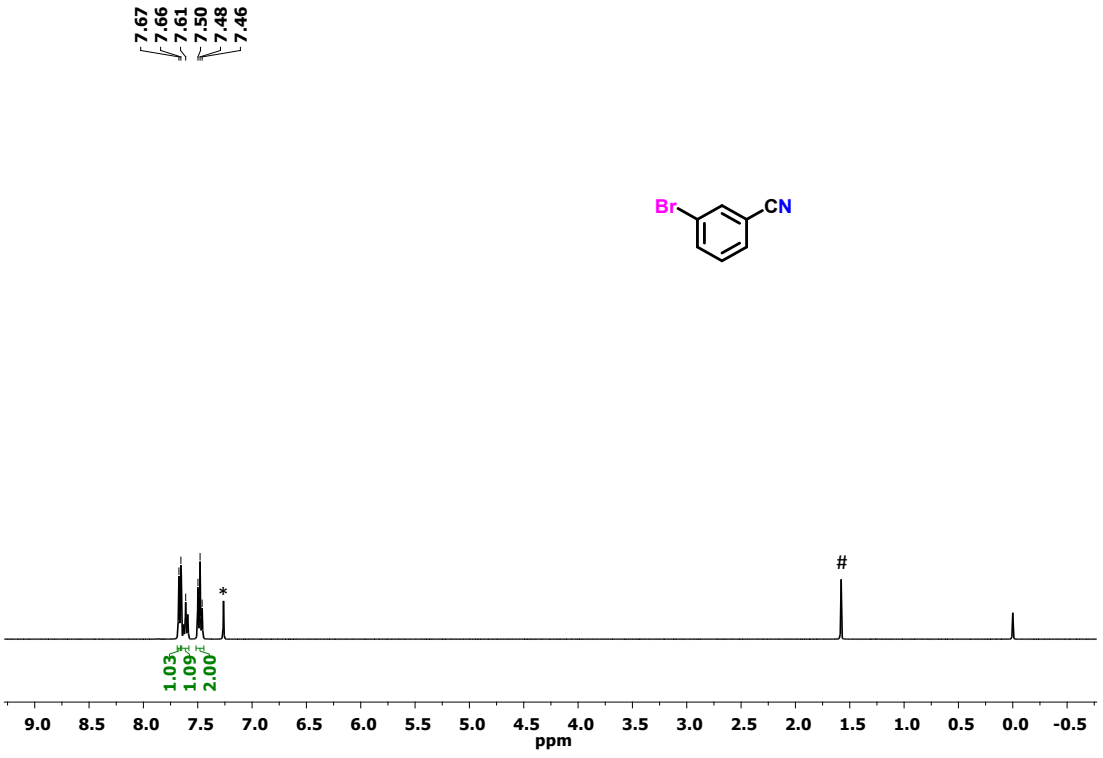

Figure S56. ^{1}H NMR spectrum of 3-bromobenzonitrile (table 3, entry 11) in $CDCl_3$. * and # represent $CDCl_3$ and H_2O peaks, respectively.

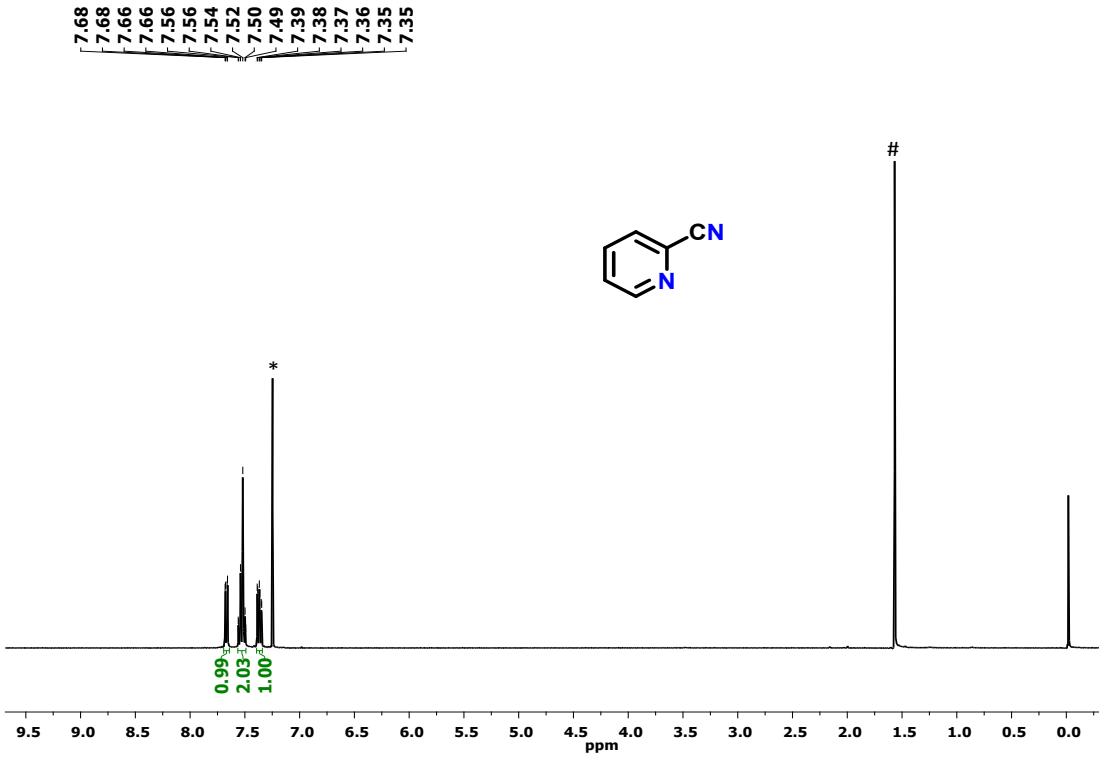

Figure S57. ^{1}H NMR spectrum of picolinonitrile (table 3, entry 12) in $CDCl_3$. * and # represent $CDCl_3$ and H_2O peaks, respectively.

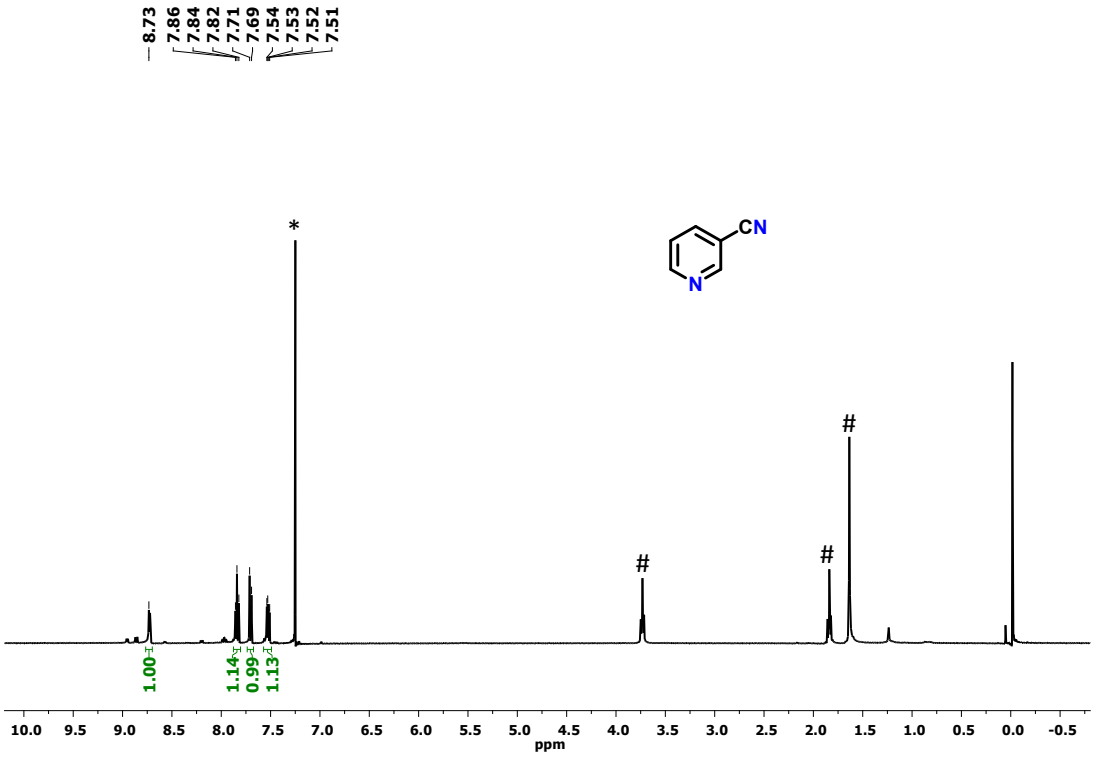

Figure S58. ^{1}H NMR spectrum of nicotinonitrile (table 3, entry 13) in $CDCl_3$. * and # represent $CDCl_3$ and H_2O/residual solvent peaks, respectively.

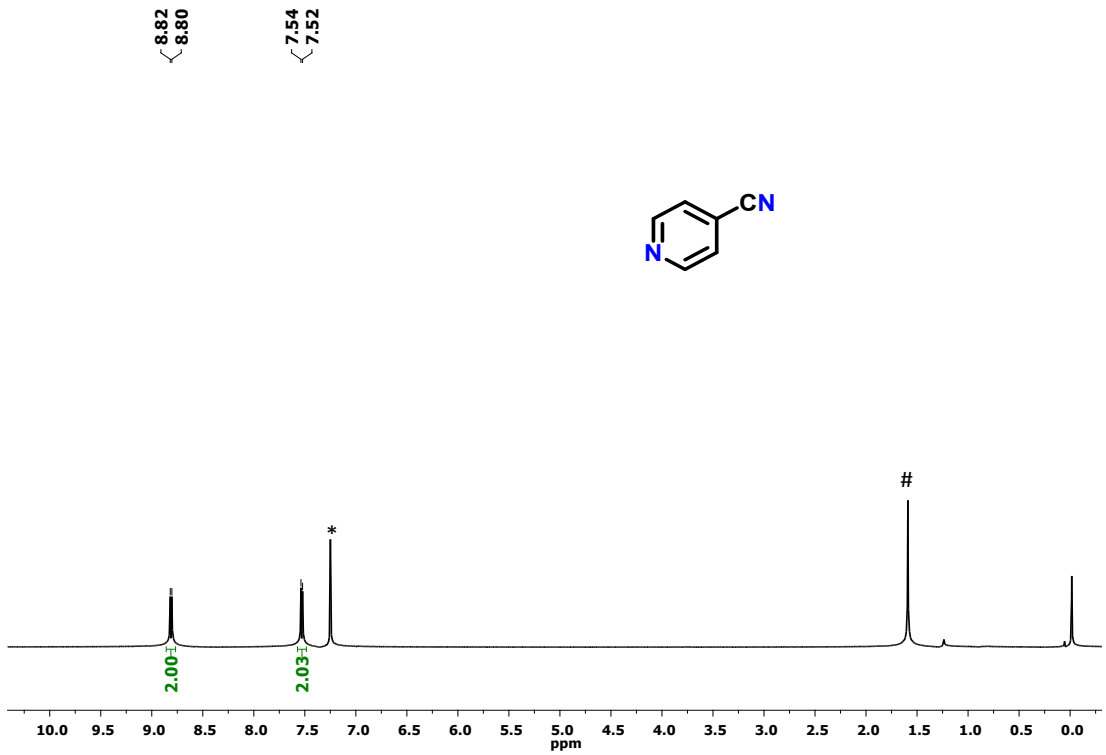

Figure S59. ^{1}H NMR spectrum of isonicotinonitrile (table 3, entry 14) in $CDCl_3$. * and # represent $CDCl_3$ and H_2O peaks, respectively.

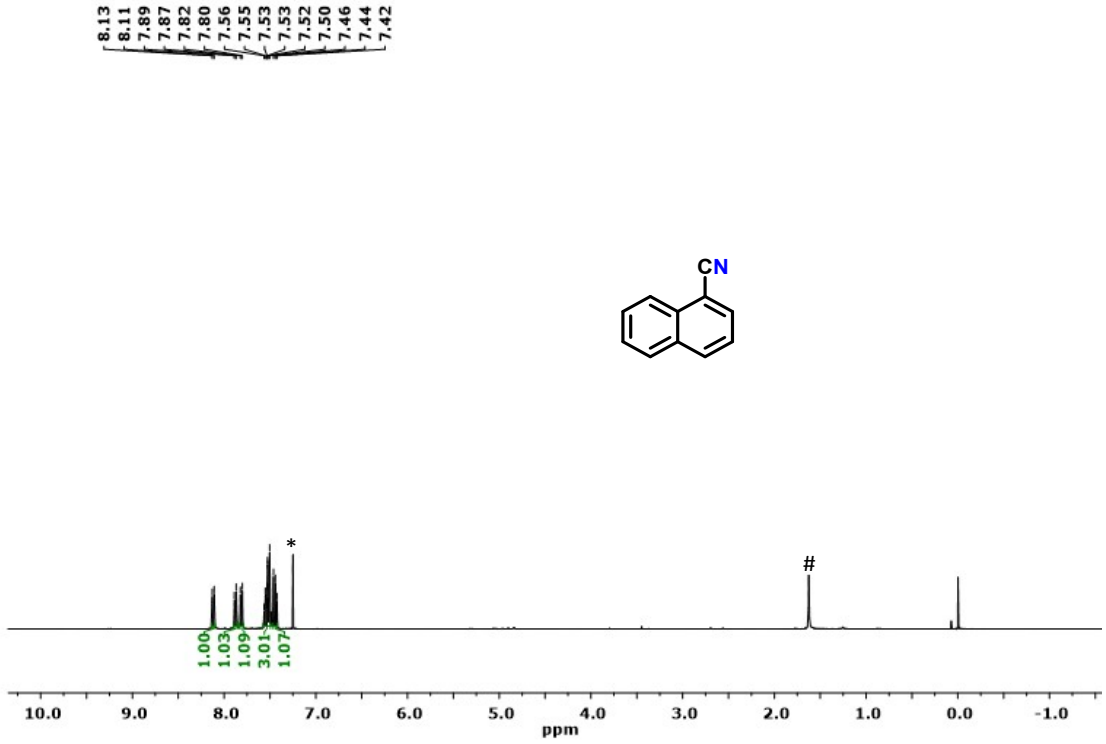

Figure S60. ^{1}H NMR spectrum of 1-naphthonitrile (table 3, entry 15) in $CDCl_3$. * and # represent $CDCl_3$ and H_2O peaks, respectively.

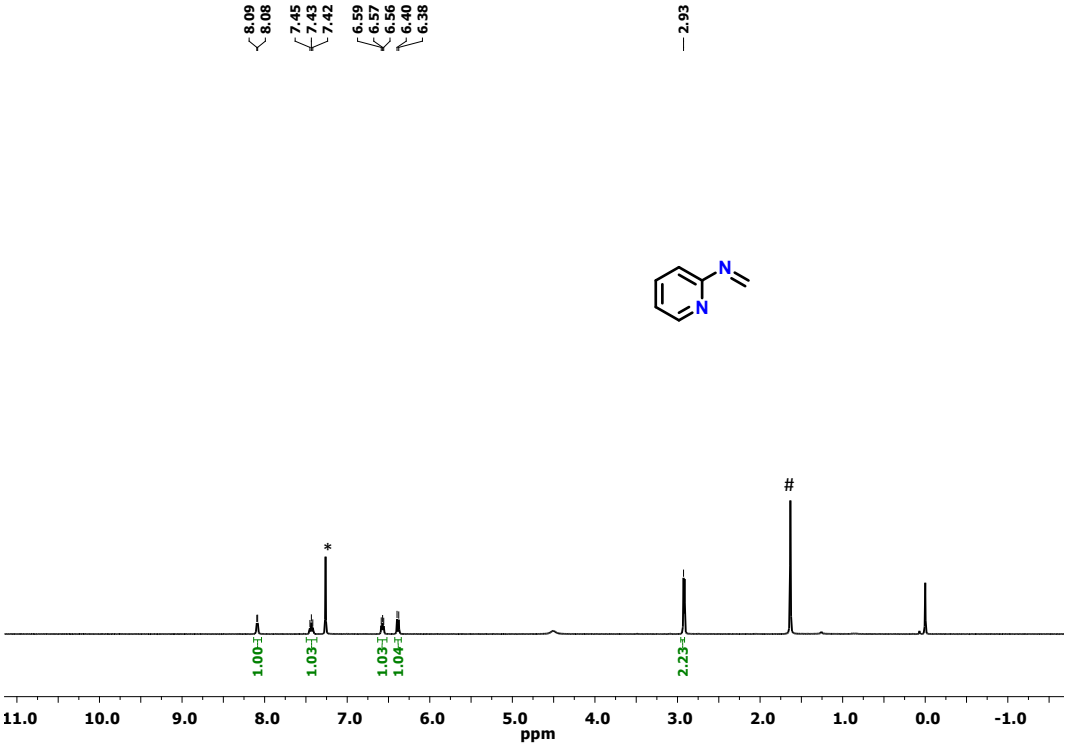

Figure S61. ^{1}H NMR spectrum of *N*-(pyridin-2-yl)methanimine (table 4, entry 1) in $CDCl_3$. * and # represent $CDCl_3$ and H_2O peaks, respectively.

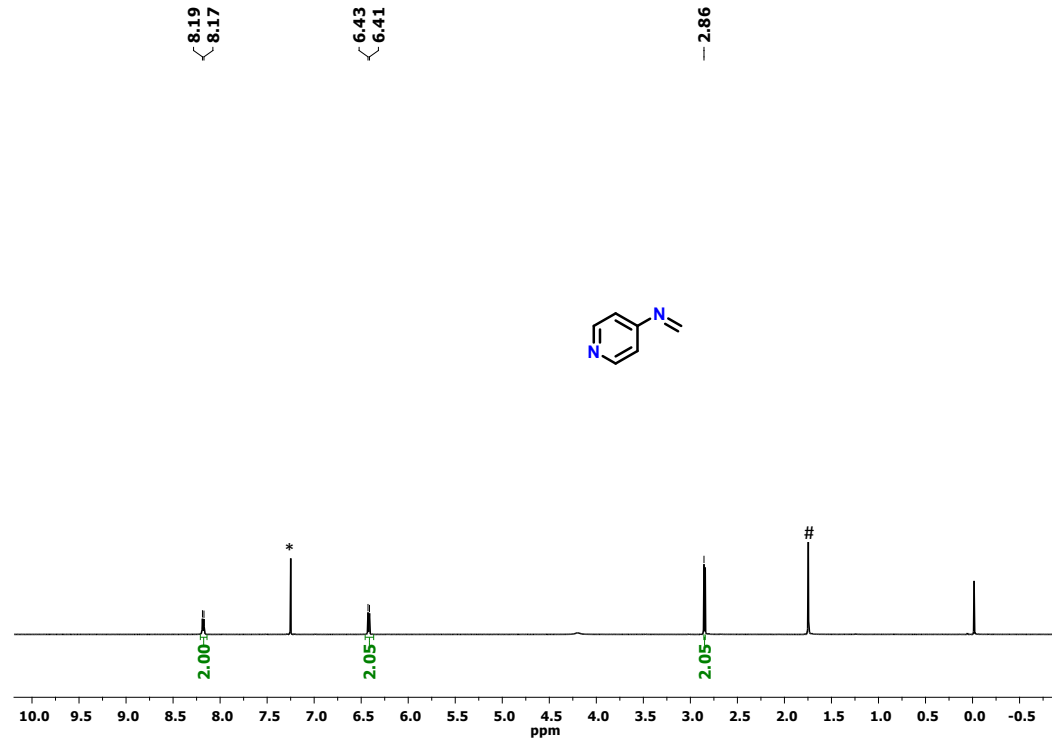

Figure S62. ^{1}H NMR spectrum of *N*-(pyridin-4-yl)methanimine (table 4, entry 2) in $CDCl_3$. * and # represent $CDCl_3$ and H_2O peaks, respectively.

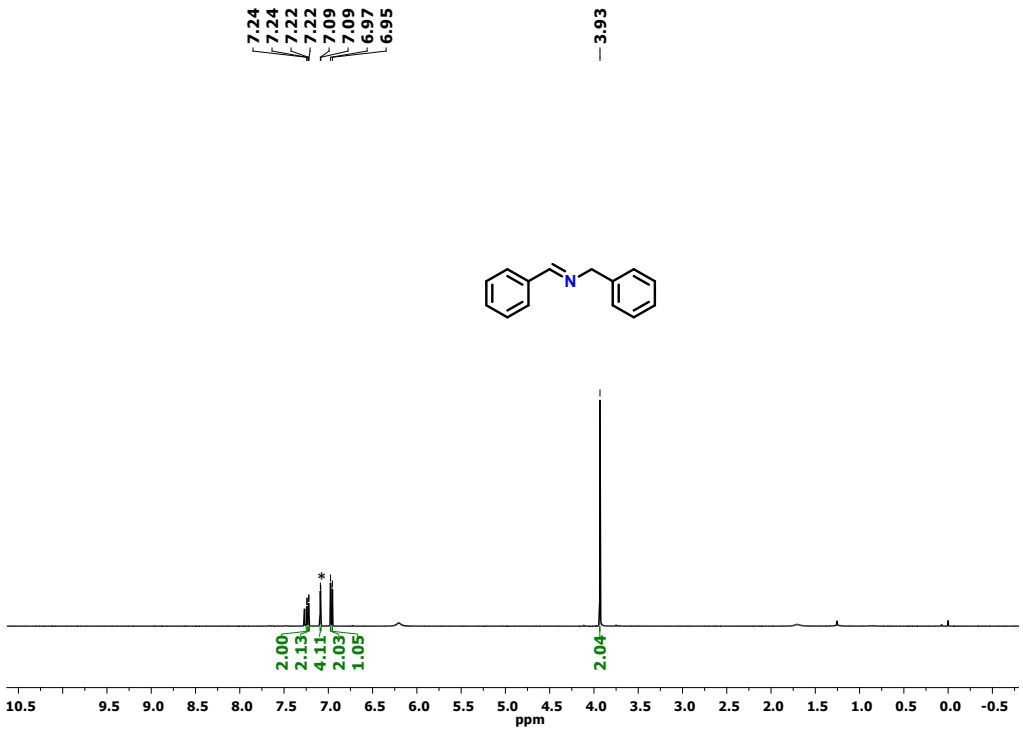

Figure S63. ^{1}H NMR spectrum of *N*-benzyl-1-phenylmethanimine (table 4, entry 7) in $CDCl_3$. * represents $CDCl_3$ peak.

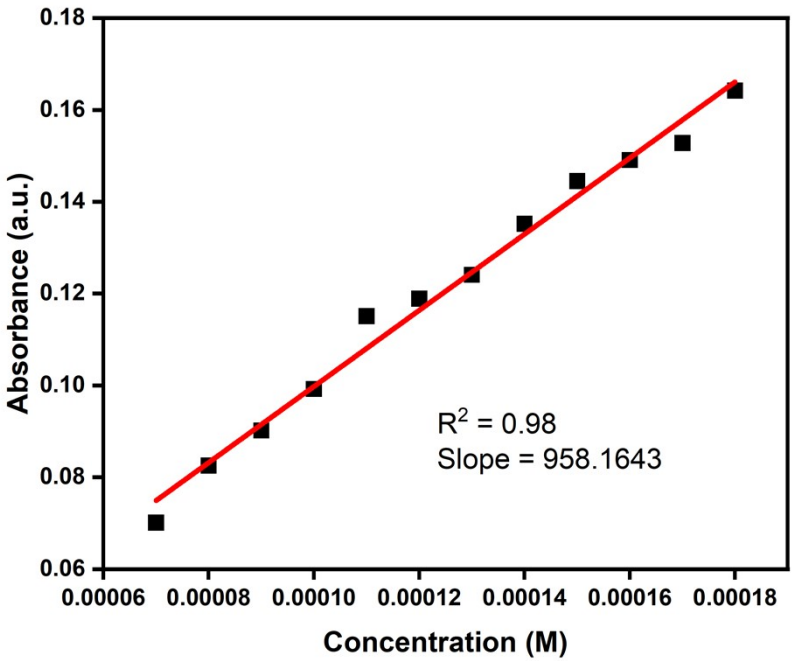

Figure S64. Plot of absorbance at λ = 400 nm against concentration for the titration of complex **2** with benzylamine.

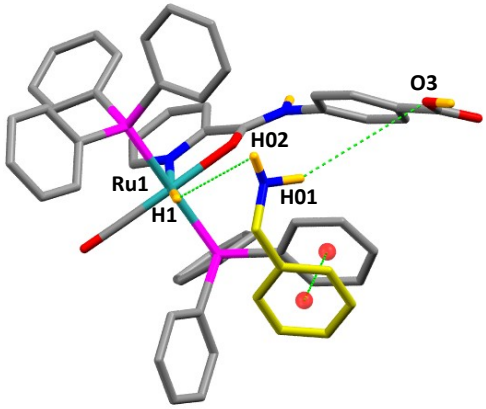

Figure S65. Molecular docking of complex **2** with a molecule of benzylamine (shown in yellow color) exhibiting hydrogen bonding, dihydrogen bonding, and $\pi_{arene}\cdots\pi_{arene}$ interactions (shown by red dots). Only selected hydrogen atoms (in orange color) are shown for clarity. Selected heteroatom separations (Å): (a) O3…N, 3.41, Ru1…N, 2.8, $\pi_{arene}\cdots\pi_{arene}$, 2.62.

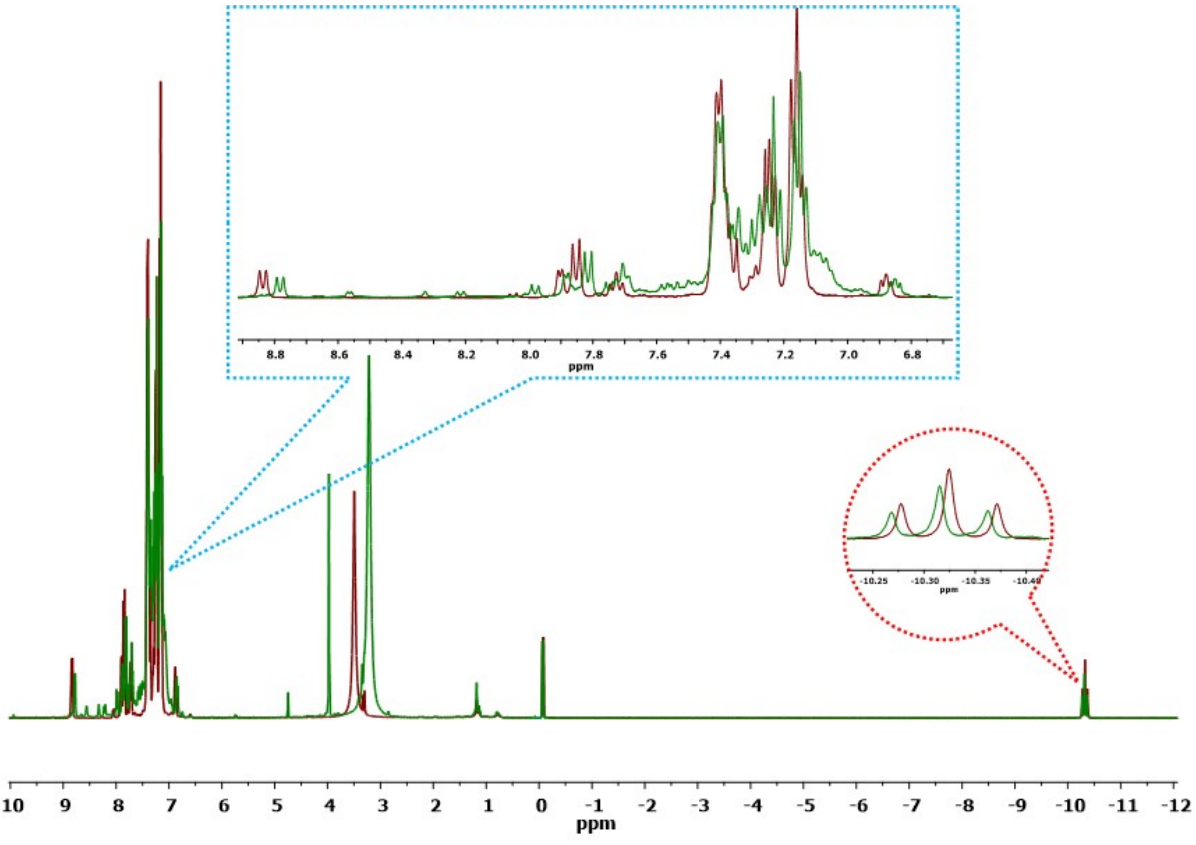

Figure S66. A comparison of ^{1}H NMR spectra of complex **2** (brown trace) and a 1:1 mixture of complex **2** + benzylamine (green trace) recorded in $CDCl_3$.

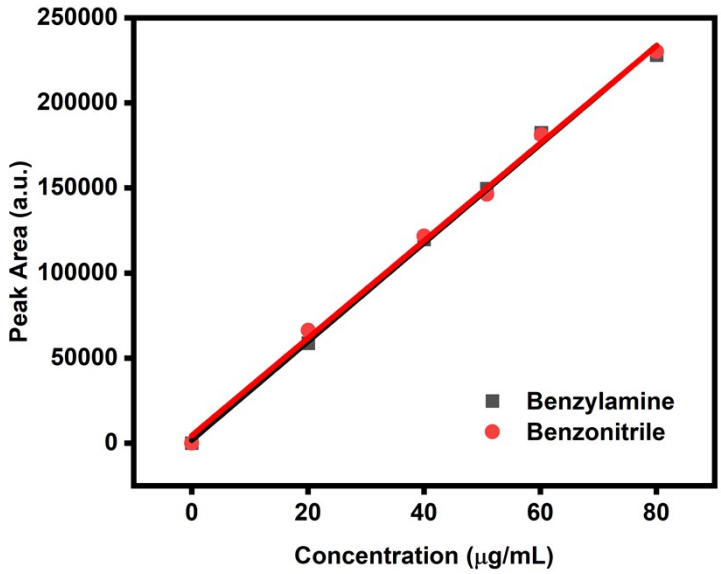

Figure S67. GC calibration plot for benzylamine and benzonitrile.

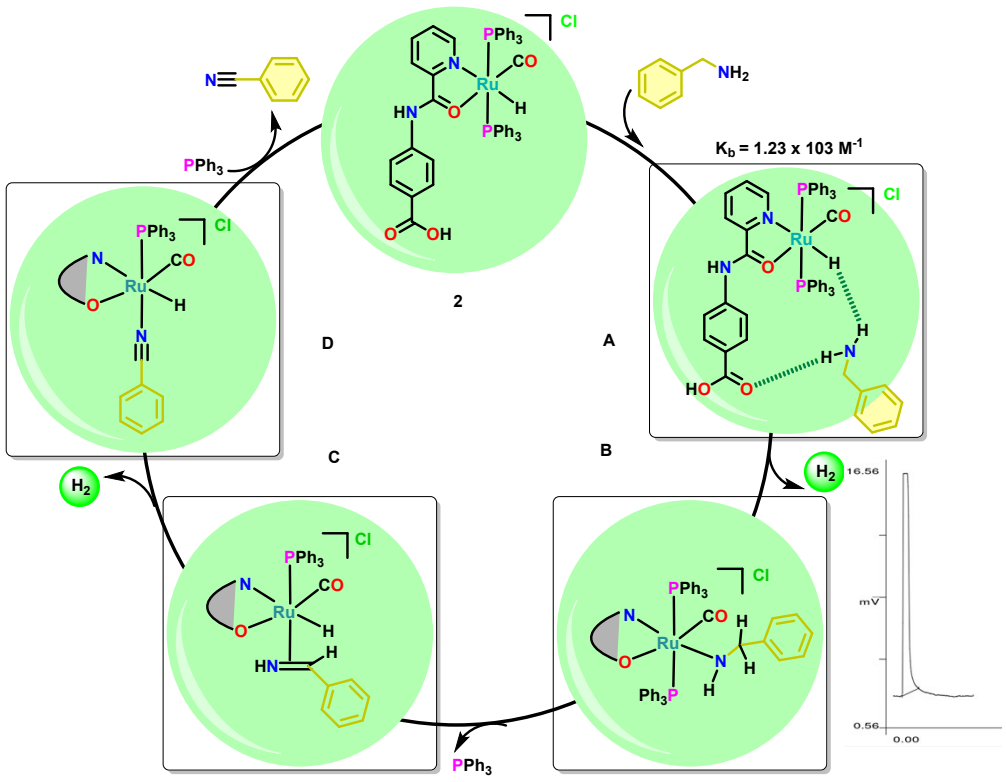

Scheme S1. Proposed reaction mechanism for the double dehydrogenation of benzylamine catalyzed by complex **2**. A gas chromatogram for the in-situ generated H_2 is shown adjacent to panel '**B**'.

Table S1. X-ray diffraction data collection and structure refinement parameters for complexes **2** and **3**.

	2·CH$_3$OH	**3·3CH$_3$OH·H$_2$O**
CCDC No.	**2402741**	**2402742**
Empirical formula	$C_{52}H_{49}N_2O_6P_2RuCl$	$C_{55}H_{59}N_2O_8P_2RuCl$
Formula weight	996.43	1073.55
Temperature (K)	293(2)	293(2)
Wavelength (Å)	0.71073	0.71073
Crystal system	Triclinic	Monoclinic
Space group	$P\bar{1}$	$P2_1/n$
a(Å)	11.3027(3)	15.0241(2)
b(Å)	12.3655(4)	19.0497(3)
c(Å)	17.0464(5)	17.0542(3)
α(°)	82.161(2)	90
β(°)	83.388(2)	97.7020(10)
γ(°)	77.112(3)	90
Volume (Å^3)	2291.87(12)	4836.96(13)
Z	2	4
Density Mg/m^3 (calculated)	1.397	1.345
Absorption coefficient mm^{-1}	0.516	0.491
F(000)	956	2008
Crystal size (mm^3)	0.24 x 0.20 x 0.16	0.25 x 0.19 x 0.16
Theta range for data collection	3.403 to 24.998°	3.116 to 27.455°
Index ranges	-13<=h<=13, -14<=k<=14, -20<=l<=20	-18<=h<=19, -24<=k<=24, -22<=l<=21
Reflections collected	27963	73595
Independent reflections	8085 [R(int) = 0.0362]	11070 [R(int) = 0.0454]
Completeness to theta = 25°	99.8 %	99.8 %
Refinement method	Full-matrix least-squares on F^2	Full-matrix least-squares on F^2
Data / restraints / parameters	8085 / 176 / 579	10535 / 932 / 563
Goodness of-fit on F^2	1.039	1.072
Final R indices [I>2sigma(I)][a,b]	R_1 = 0.0416, wR_2 = 0.0966	R_1 = 0.0315, wR_2 = 0.0824
R indices (all data)	R_1 = 0.0493, wR_2 = 0.1004	R_1 = 0.0405, wR_2 = 0.0859
Largest diff. peak and hole (e.Å^{-3})	1.081 and -0.607	0.382 and -0.437

[a] $R = \Sigma||F_o| - |F_c||/\Sigma|F_o|$; [b] $wR = \{\Sigma[w(F_o^2 - F_c^2)^2]/\Sigma[wF_o^4]\}^{1/2}$

Table S2. Selected bond distances (Å) and bond angles (°) for complexes **2** and **3**.

Bond Length (Å)	**2**	**3**
Ru(1)-C(1)	1.843(4)	1.800(2)
Ru(1)-N(1)	2.175(2)	2.174(15)
Ru(1)-O(1)	2.153(2)	2.164(11)
Ru(1)-P(1)	2.3584(8)	2.3579(5)
Ru(1)-P(2)	2.3460(8)	2.3565(5)
Ru(1)-H(1)	1.619(10)	1.621(16)

Bond Angles (°)	**2**	**3**
C(1)-Ru(1)-O(1)	172.52(12)	173.49(7)
C(1)-Ru(1)-N(1)	98.54(13)	99.38(8)
O(1)-Ru(1)-N(1)	74.19(8)	74.16(5)
C(1)-Ru(1)-P(1)	89.54(11)	92.69(7)
O(1)-Ru(1)-P(1)	89.31(6)	88.76(3)
N(1)-Ru(1)-P(1)	94.51(7)	94.96(4)
C(1)-Ru(1)-P(2)	91.01(11)	92.01(7)
O(1)-Ru(1)-P(2)	91.11(6)	87.69(3)
N(1)-Ru(1)-P(2)	92.95(7)	94.06(4)
P(1)-Ru(1)-P(2)	172.36(3)	169.016(19)
C(1)-Ru(1)-H(1)	91.6(15)	86.4(6)
O(1)-Ru(1)-H(1)	95.9(15)	100.0(6)
N(1)-Ru(1)-H(1)	167.0(15)	174.2(6)
P(1)-Ru(1)-H(1)	93.8(16)	85.5(5)
P(2)-Ru(1)-H(1)	78.6(15)	84.9(6)

Table S3. Calculation of extinction coefficient using the concentration and absorbance at λ = 400 nm for the titration of complex **2** with benzylamine.

S.No.	Concentration (M)*10^{-6}	Absorbance (a.u.)	Extinction Coefficient, ε (M^{-1} cm^{-1})
1	70	0.07011	1001.57
2	80	0.08254	1031.75
3	90	0.09021	1003.33
4	100	0.09923	992.3
5	110	0.1151	1046.36
6	120	0.1189	990.83
7	130	0.1241	954.61
8	140	0.1352	965.71
9	150	0.1445	963.33
10	160	0.1491	931.87
11	170	0.1528	898.82
12	180	0.1642	911.66

Table S4. Computational data for the molecular docking studies of complex **2** with a molecule of benzylamine.

Clst	E_{total}	E_{shape}	E_{force}	E_{air}	Bmp	RMS
1	-126.4	-126.4	0.0	0.0	1	1.00

REMARK Docked receptor coordinates...
REMARK model "benzylamine", ID: 004a011a00080006

HETATM	1	N	1	1.928	1.675	0.265	1.00	99.99
HETATM	2	C	1	1.223	1.096	-0.887	1.00	99.99
HETATM	3	C	1	0.212	0.089	-0.391	1.00	99.99
HETATM	4	C	1	0.413	-1.233	-0.537	1.00	99.99
HETATM	5	C	1	-0.491	-2.120	-0.092	1.00	99.99
HETATM	6	C	1	-1.612	-1.693	0.507	1.00	99.99
HETATM	7	C	1	-1.824	-0.377	0.659	1.00	99.99
HETATM	8	C	1	-0.916	0.505	0.212	1.00	99.99
HETATM	9	H	1	2.462	2.514	-0.020	1.00	99.99
HETATM	10	H	1	1.238	2.009	0.961	1.00	99.99
HETATM	11	H	1	1.963	0.642	-1.586	1.00	99.99
HETATM	12	H	1	0.702	1.909	-1.443	1.00	99.99
HETATM	13	H	1	1.331	-1.601	-1.025	1.00	99.99
HETATM	14	H	1	-0.311	-3.201	-0.218	1.00	99.99
HETATM	15	H	1	-2.356	-2.420	0.874	1.00	99.99
HETATM	16	H	1	-2.744	-0.020	1.152	1.00	99.99
HETATM	17	H	1	-1.102	1.584	0.344	1.00	99.99

REMARK Docked ligand coordinates...
REMARK model "complex 2", ID: 004a011a00080006

HETATM	18	Ru1	UNK	1	4.605	-1.471	1.290	1.00	2.58
HETATM	19	P2	UNK	1	6.430	-0.098	0.751	1.00	2.55
HETATM	20	P1	UNK	1	2.611	-2.691	1.613	1.00	2.67
HETATM	21	O2	UNK	1	4.004	-0.129	2.862	1.00	2.83
HETATM	22	N2	UNK	1	3.685	0.106	5.082	1.00	3.06
HETATM	23	H6	UNK	1	3.925	-0.145	5.868	1.00	3.63
HETATM	24	O4	UNK	1	-0.339	4.795	3.654	1.00	5.88
HETATM	25	H7	UNK	1	-0.991	5.292	3.634	1.00	8.84
HETATM	26	N1	UNK	1	5.556	-2.215	3.098	1.00	2.74
HETATM	27	O3	UNK	1	-1.419	3.927	5.377	1.00	6.88
HETATM	28	C10	UNK	1	2.795	2.138	4.051	1.00	3.15
HETATM	29	H10	UNK	1	3.543	2.194	3.502	1.00	3.79
HETATM	30	C11	UNK	1	1.790	3.078	3.950	1.00	3.17
HETATM	31	H11	UNK	1	1.862	3.770	3.334	1.00	3.79
HETATM	32	C45	UNK	1	1.157	-1.745	2.179	1.00	3.06
HETATM	33	C12	UNK	1	0.668	2.992	4.769	1.00	3.28
HETATM	34	C27	UNK	1	7.923	-0.565	1.663	1.00	2.71
HETATM	35	C9	UNK	1	2.683	1.107	4.973	1.00	2.96
HETATM	36	C23	UNK	1	6.981	-0.098	-1.004	1.00	3.00
HETATM	37	C33	UNK	1	1.948	-3.619	0.173	1.00	3.12
HETATM	38	O1	UNK	1	5.584	-3.591	-0.574	1.00	6.02
HETATM	39	C15	UNK	1	6.174	1.686	1.047	1.00	3.30
HETATM	40	C38	UNK	1	2.272	-3.221	-1.106	1.00	3.64
HETATM	41	H38	UNK	1	2.860	-2.511	-1.235	1.00	4.34
HETATM	42	C50	UNK	1	1.105	-0.376	2.031	1.00	3.35

	HETATM 43 H50 UNK 1 1.838 0.066 1.665 1.00 4.03 HETATM 44 C37 UNK 1 1.721 -3.878 -2.209 1.00 4.29 HETATM 45 H37 UNK 1 1.948 -3.607 -3.071 1.00 5.13 HETATM 46 C7 UNK 1 4.273 -0.461 4.034 1.00 2.72 HETATM 47 C26 UNK 1 7.774 0.053 -3.660 1.00 4.72 HETATM 48 H26 UNK 1 8.033 0.110 -4.551 1.00 5.68 HETATM 49 C5 UNK 1 7.087 -3.556 4.328 1.00 4.81 HETATM 50 H3 UNK 1 7.697 -4.258 4.340 1.00 5.76 HETATM 51 C34 UNK 1 1.069 -4.664 0.331 1.00 4.30 HETATM 52 H34 UNK 1 0.833 -4.945 1.185 1.00 5.13 HETATM 53 C13 UNK 1 0.596 1.981 5.716 1.00 4.13 HETATM 54 H13 UNK 1 -0.138 1.934 6.287 1.00 4.97 HETATM 55 C28 UNK 1 8.195 -0.054 2.924 1.00 3.53 HETATM 56 H28 UNK 1 7.675 0.636 3.269 1.00 4.26 HETATM 57 C42 UNK 1 3.708 -5.735 4.826 1.00 13.72 HETATM 58 H42 UNK 1 3.995 -6.332 5.481 1.00 16.50 HETATM 59 C39 UNK 1 2.864 -3.962 2.873 1.00 4.30 HETATM 60 C20 UNK 1 7.221 2.560 1.222 1.00 4.51 HETATM 61 H20 UNK 1 8.092 2.238 1.260 1.00 5.45 HETATM 62 C21 UNK 1 6.186 -0.621 -2.004 1.00 4.06 HETATM 63 H21 UNK 1 5.375 -1.021 -1.788 1.00 4.82 HETATM 64 C36 UNK 1 0.862 -4.908 -2.035 1.00 4.59 HETATM 65 H36 UNK 1 0.497 -5.342 -2.773 1.00 5.53 HETATM 66 C22 UNK 1 8.189 0.499 -1.357 1.00 3.89 HETATM 67 H22 UNK 1 8.743 0.852 -0.699 1.00 4.66 HETATM 68 C6 UNK 1 6.445 -3.221 3.161 1.00 3.62 HETATM 69 H2 UNK 1 6.634 -3.704 2.388 1.00 4.34 HETATM 70 C3 UNK 1 5.901 -1.831 5.425 1.00 4.16 HETATM 71 H5 UNK 1 5.706 -1.337 6.189 1.00 4.97 HETATM 72 C32 UNK 1 8.703 -1.606 1.180 1.00 3.66 HETATM 73 H32 UNK 1 8.524 -1.966 0.340 1.00 4.42 HETATM 74 C24 UNK 1 6.591 -0.551 -3.328 1.00 4.88 HETATM 75 H24 UNK 1 6.055 -0.917 -3.995 1.00 5.84 HETATM 76 C2 UNK 1 5.281 -1.549 4.237 1.00 2.86 HETATM 77 C25 UNK 1 8.566 0.569 -2.690 1.00 4.44 HETATM 78 H25 UNK 1 9.372 0.974 -2.921 1.00 5.29 HETATM 79 C30 UNK 1 10.024 -1.589 3.166 1.00 4.89 HETATM 80 H30 UNK 1 10.741 -1.915 3.659 1.00 5.84 HETATM 81 C8 UNK 1 1.606 1.039 5.819 1.00 3.85 HETATM 82 H8 UNK 1 1.556 0.366 6.459 1.00 4.66 HETATM 83 C31 UNK 1 9.747 -2.115 1.941 1.00 4.65 HETATM 84 H31 UNK 1 10.261 -2.818 1.613 1.00 5.61 HETATM 85 C49 UNK 1 -0.002 0.356 2.408 1.00 4.68 HETATM 86 H49 UNK 1 -0.018 1.280 2.295 1.00 5.61 HETATM 87 C1 UNK 1 5.200 -2.771 0.110 1.00 3.83 HETATM 88 C14 UNK 1 -0.469 3.946 4.646 1.00 3.97 HETATM 89 C29 UNK 1 9.243 -0.572 3.677 1.00 4.66 HETATM 90 H29 UNK 1 9.418 -0.232 4.525 1.00 5.61 HETATM 91 C16 UNK 1 4.876 2.197 1.009 1.00 4.00 HETATM 92 H16 UNK 1 4.159 1.615 0.902 1.00 4.82 HETATM 93 C4 UNK 1 6.824 -2.856 5.473 1.00 5.27 HETATM 94 H4 UNK 1 7.258 -3.066 6.267 1.00 6.32 HETATM 95 C35 UNK 1 0.532 -5.302 -0.779 1.00 5.06 HETATM 96 H35 UNK 1 -0.060 -6.009 -0.661 1.00 6.08 HETATM 97 C47 UNK 1 -1.058 -1.653 3.113 1.00 6.41 HETATM 98 H47 UNK 1 -1.793 -2.087 3.482 1.00 7.66 HETATM 99 C46 UNK 1 0.057 -2.386 2.726 1.00 4.89 HETATM 100 H46 UNK 1 0.065 -3.309 2.833 1.00 5.84 HETATM 101 C48 UNK 1 -1.076 -0.293 2.951 1.00 6.12 HETATM 102 H48 UNK 1 -1.825 0.192 3.213 1.00 7.34 HETATM 103 C19 UNK 1 6.976 3.940 1.342 1.00 6.10 HETATM 104 H19 UNK 1 7.683 4.534 1.450 1.00 7.34

	HETATM 105 C40 UNK 1 3.499 -5.121 2.516 1.00 6.84 HETATM 106 H40 UNK 1 3.667 -5.305 1.620 1.00 8.21 HETATM 107 C17 UNK 1 4.640 3.547 1.123 1.00 5.33 HETATM 108 H17 UNK 1 3.770 3.873 1.083 1.00 6.40 HETATM 109 C18 UNK 1 5.680 4.402 1.297 1.00 6.39 HETATM 110 H18 UNK 1 5.515 5.313 1.387 1.00 7.66 HETATM 111 C44 UNK 1 2.670 -3.669 4.199 1.00 6.73 HETATM 112 H44 UNK 1 2.253 -2.878 4.457 1.00 8.05 HETATM 113 C41 UNK 1 3.890 -6.016 3.490 1.00 11.95 HETATM 114 H41 UNK 1 4.284 -6.820 3.242 1.00 14.37 HETATM 115 C43 UNK 1 3.118 -4.600 5.160 1.00 11.11 HETATM 116 H43 UNK 1 2.993 -4.407 6.060 1.00 13.34 HETATM 117 H1 UNK 1 3.918 -0.404 -0.132 1.00 -0.08 HETATM 118 Cl1 UNK 1 3.780 -0.997 8.113 1.00 5.76